รายงานวิจัยฉบับสมบูรณ์

ผลของแคทไอออนที่มีต่อ $LaFe_{0.8}Co_{0.2}O_{3-x}$ และ LSGM สำหรับใช้เป็นอิเล็กโทรไลต์ในเซลล์เชื้อเพลิง

สุทิน คูหาเรืองรอง

10 มีนาคม 2547

สัญญาเลขที่ RSA/09/2544

รายงานวิจัยฉบับสมบูรณ์

ผลของแคทไอออนที่มีต่อ $LaFe_{0.8}Co_{0.2}O_{3-x}$ และ LSGM สำหรับใช้เป็นอิเล็กโทรไลต์ในเซลล์เชื้อเพลิง

ร.ศ. ดร. สุทิน คูหาเรืองรอง
วิศวกรรมเซรามิก สำนักวิชาวิศวกรรมศาสตร์
มหาวิทยาลัยเทคโนโลยีสุรนารี

สนับสนุนโดยสำนักงานกองทุนสนับสนุนการวิจัย

Acknowledgments

I would like to express my sincere gratitude to Thailand Research Fund for financial support under contract no. RSA/09/2544 for all 3 years project. Special thanks go to Dr. Sumittra Charojrochkul for her valuable advice and also Dr. Pavadee Aungkavattana and Hataithip Mahaudom for their help in CIP and XRD measurements.

Project Code: RSA448009

รหัสโครงการ RSA448009

Project Title: Effect of Cation Dopants on $LaFe_{0.8}Co_{0.2}O_{3-x}$ and LSGM as an electrolyte in SOFC

ชื่อโครงการ ผลของแคทไอออนที่มีต่อ $LaFe_{0.8}Co_{0.2}O_{3-x}$ และ LSGM สำหรับใช้เป็นอิเล็กโทรไลต์ในเซลล์เชื้อเพลิง

Investigator: Sutin Kuharuangrong

นักวิจัย สุทิน คูหาเรืองรอง

Institute: School of Ceramic Engineering, Suranaree University of Technology

สถาบัน วิศวกรรมเซรามิก สำนักวิชาวิศวกรรมศาสตร์ มหาวิทยาลัยเทคโนโลยีสุรนารี

E-mail address: sutin@ccs.sut.ac.th

Project Period: 3 years (January 15, 2001 – January 14, 2004)

ระยะเวลาโครงการ 3 ปี (15 มกราคม พ.ศ. 2544 – 14 มกราคม พ.ศ. 2547)

บทคัดย่อ

งานวิจัยนี้มุ่งที่จะลดอุณหภูมิใช้งานของสารอิเล็กโทรไลต์ในเซลล์เชื้อเพลิงออกไซด์ของแข็ง ส่วนผสมที่ถูกเลือกใช้เป็นตัวหลักของโครงงานวิจัยนี้ คือ $La_{1-x}Sr_xGa_{1-y}Mg_yO_{3-\delta}$ (LSGM), $La_{1-x}Sr_xCo_{1-y}Fe_yO_{3-\delta}$ (LSCF) และ CeO_2 โดยทำการเลือกสารเติมที่มีประจุที่ต่ำกว่าและมีขนาดที่ใกล้เคียงกับแคทไอออนที่จะถูกแทนที่ ปริมาณของสารเติมถูกปรับเปลี่ยนและทำการตรวจสอบเฟสโดยใช้วิธีการเลี้ยวเบนของรังสีเอกซ์ ตรวจสอบจุลโครงสร้างเพื่อดูขนาดของอนุภาคโดยใช้กล้องจุลทรรศน์แบบส่องกวาด ตรวจสอบค่าการนำไฟฟ้าด้วยวิธี dc 4-points และ ac impedance โดยวัดที่อุณหภูมิต่าง ๆ กัน สำหรับการตรวจสอบ ac impedance ทำการเก็บข้อมูลที่ความถี่ต่าง ๆ กัน และในสภาวะต่าง ๆ กัน เช่น ในอากาศปกติ ในออกซิเจน และในคาร์บอนมอนอกไซด์ นอกจากนี้ CeO_2 ที่ถูกเติมด้วยสารบางตัวถูกตรวจสอบความเสถียรโดยดูจากค่า impedance ที่เปลี่ยนไปหลังจากถูกเผาแช่ที่อุณหภูมิ 700 องศาเซลเซียส เป็นเวลา 90 ชั่วโมงในบรรยากาศออกซิเจน

ผลการทดสอบปรากฏว่าสาร LSGM ที่เตรียมขึ้นไม่เสถียรและยากที่จะเตรียมขึ้นให้ได้เหมือนเดิม จากการตรวจสอบด้วยวิธีการเลี้ยวเบนของรังสีเอกซ์มักพบเฟสอื่นหลังทำการเผาแคลไซน์ ในบางครั้งจึงจำเป็นต้องเผาซ้ำที่อุณหภูมิสูงกว่าเดิม สำหรับ LSCF หลังเผาแคลไซน์และเผาผนึกพบเพียงเฟสของ LSCF เพียงเฟสเดียว แต่ในระหว่างการเผาผนึกพบสีน้ำเงินของโคบอลท์ปรากฏอยู่บนแผ่นรองเผาและสีน้ำเงินบนแผ่นรองเผาจะเข้มมากขึ้นถ้าสาร LSCF มีส่วนผสมของปริมาณโคบอลท์เพิ่มขึ้น

สำหรับ CeO_2 พบว่าสารเติมสามารถถูกผสมได้ถึง 30 โมลเปอร์เซนต์ใน CeO_2 โดยที่ยังคงได้เฟสเดียว และเมื่อปริมาณของสารเติมเพิ่มขึ้นจะช่วยลดค่าอิมพีแดนซ์ของ CeO_2 สำหรับการโตของอนุภาคของ CeO_2 ขึ้นกับชนิดของสารเติม สำหรับงานวิจัยนี้ได้เลือกสาร rare-earth เป็นสารเติมแต่งและจากผลทดลองพบว่า Sm ให้ผลในการลดค่าอิมพีแดนซ์ได้ดีที่สุด รองลงมาคือ Gd, Dy, Er และ Y เรียงลงมาตามลำดับ

สำหรับผลของบรรยากาศที่มีต่อค่าอิมพีแดนซ์พบว่าถ้าทำการตรวจสอบในบรรยากาศออกซิเจนค่าความแตกต่างระหว่างอิมพีแดนซ์ที่พบใน bulk กับที่พบที่ขอบเกรน (grain boundary) จะมีค่าความต่างน้อยลงเมื่อเทียบกับในบรรยากาศปกติ ในตัวอย่างของ CeO_2 ที่มีสารเติมแต่งบางตัวที่ถูกนำไปเผาแช่ที่อุณหภูมิ 700 องศาเซลเซียส เป็นเวลา 90 ชั่วโมงในบรรยากาศออกซิเจน พบว่าค่าอิมพีแดนซ์เปลี่ยนไปจากเดิม

คำหลัก ซีเรียมออกไซด์
อิเล็กโทรไลต์สำหรับเซลล์เชื้อเพลิงออกไซด์ของแข็ง
การวัดค่าอิมพีแดนซ์

Abstract

The objective of this project is to reduce the operating temperature of SOFC electrolyte. The selected base materials are $La_{1-x}Sr_xGa_{1-y}Mg_yO_{3-\delta}$ (LSGM), $La_{1-x}Sr_xCo_{1-y}Fe_yO_{3-\delta}$ (LSCF) and CeO_2. The choice of cation dopants is based on the lower charge and comparable size as compared to the substituted cation. The phase detected by XRD and the microstructure revealed by SEM determine the phase present and grain size with varying amount of dopants. The electrical conductivities, dc 4-points and ac impedance measurements are examined as a function of temperature. In addition, ac impedance measurements are investigated as a function of frequency in different atmospheres, i.e. air, oxygen and carbon monoxide. The stability after operating for 90 hrs. at 700 ^{o}C of some doped ceria is studied to observe a change of impedance.

The results show that LSGM is unstable and difficult to reproduce. The second phase detected by XRD is found in calcined LSGM powder. Recalcination at higher temperature is required to remove the other phase. In contrast, the single phase of LSCF can be obtained after calcination and sintering. However, the diffusion of Co from the materials to the substrate cannot be controlled during sintering. Also, the strong blue color on the substrate is found from the composition with higher amount of Co.

The results of rare-earth cations doped into CeO_2 indicate that only single phase of ceria can be existed within 30 mol% dopant. An increasing amount of dopant reduces the impedance of ceria although the growth of grain depends upon the type of dopants. The most effective dopants determined from their influence on the lowest impedance are found in the following order; Sm > Gd > Dy > Er > Y.

The effect of atmosphere on the impedance of ceria shows that oxygen can reduce the difference between bulk and grain boundary impedances as compared to the measurement in air. Moreover, the impedance of doped ceria can be altered after operating at 700 ^{o}C for 90 hrs in oxygen.

Keywords CeO_2

SOFC electrolyte

Impedance measurement

TABLE OF CONTENTS

List of Tables

List of Figures

Introduction

When the high-efficiency power generation and pollution control are addressed, fuel cell is one of the most interesting and promising technologies in the 21st century. It is an environmentally clean, quiet and highly efficient method for generating electricity and heat directly from a variety of fuels without conversion of chemical energy of fuel into thermal and mechanical energies, as a bypass.

There are several types of fuel cells currently under development, alkaline fuel cell (AFC), phosphoric acid fuel cell (PAFC), proton exchanged membrane fuel cell (PEMFC), molten carbonate fuel cell (MCFC) and solid oxide fuel cell (SOFC).

In this project, only SOFC is concentrated to be developed for an intermediate operating temperature since the other fuel cells can be worked at lower than 650 °C. Although at the high operating temperature, the external reformer, air compressor and catalysts are not required, the material selection is limited and material compatibility can be a serious problem.

A single SOFC consists of a solid oxide electrolyte sandwiched between two electrodes, anode and cathode. Each component must have the proper stability (i.e. phase and dimension) in oxidizing and/or reducing environments, chemical compatibility and proper conductivity with other components.

Yttria-stabilized zirconia (YSZ) is the most common electrolyte used in commercial SOFC because it possesses an adequate level of oxygen-ion conductivity and exhibits desirable stability in both oxidizing and reducing atmospheres. However, the high operating temperature of 1000 °C is required for bulk material and 850 °C for thin sheet of YSZ. To reduce this operating temperature, the alternative electrolyte materials should be proposed and studied.

The objectives of this project are:

1. To synthesize the other electrolyte materials to operate at lower temperatures (~700-850 °C)

2. To investigate the electrical conductivity of the synthesized materials in reducing and oxidizing atmospheres
3. To study the stabilities of microstructure and phase after operating for a certain period of time

Previous Work

In the first year of this project, $LaGaO_3$ and $La_{1-x}Sr_xCo_{1-y}Fe_yO_{3-\delta}$ (LSCF) were selected as alternative electrolyte materials. $LaGaO_3$, one of the promising candidates of low-temperature electrolyte materials, has been intensively studied in Japan and Europe. Sr and Mg partially doped into La-site and Ga-site respectively showed the good ionic conductivity due to increasing amount of oxygen vacancies. The optimized composition in $La_{1-x}Sr_xGa_{1-y}Mg_yO_{3-\delta}$ (LSGM) with the highest bulk conductivity of 0.17 S/cm at 800 °C was reported at x=0.20 and y=0.17 [1]. This composition remained a single phase without any grain-boundary contribution in the impedance spectrum. The contour plot of the bulk conductivity at 800 °C for this composition is shown in Fig. 1.

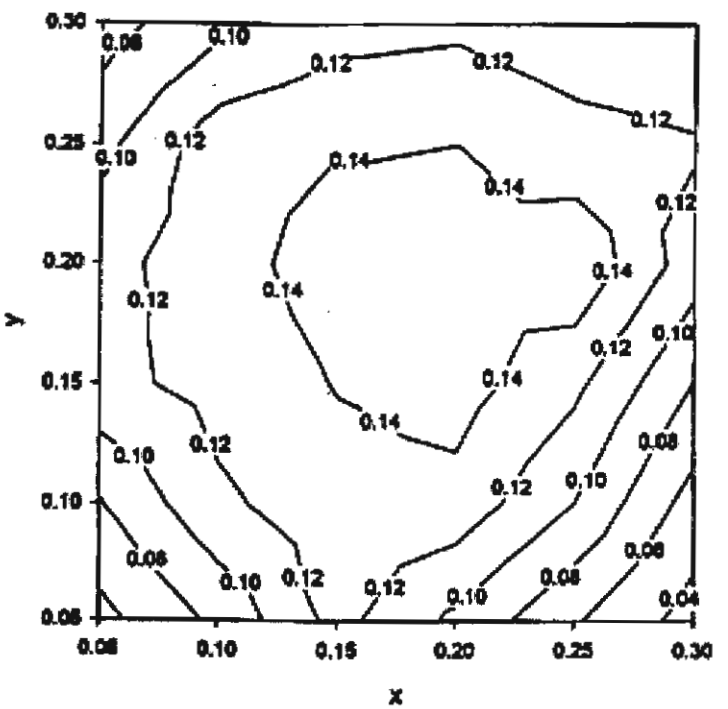

Fig. 1 Bulk conductivity of $La_{1-x}Sr_xGa_{1-y}Mg_yO_{3-\delta}$ measured at 800 °C in air (the unit is S/cm) [1]

In addition, the effects of Fe and Co were investigated in LSGM [2]. Their structures and activation energies (E_a) of these doped compositions were studied and listed in Table 1.

Table 1. Spectrum from XRD data and activation energies (E_a) of the doped LSGM [2]

Composition	Prep. T (C) air	Structure	Temperature Range (C)	E_a (eV)
$La_{0.9}Sr_{0.1}Ga_{0.8}Mg_{0.2}O_{3-\delta}$	1450	Cubic	450-620	0.981
			700-1000	0.727
$La_{0.9}Sr_{0.1}(Ga_{0.9}Fe_{0.1})_{0.8}Mg_{0.2}O_{3-\delta}$	1450	Cubic	450-1000	0.657
$La_{0.9}Sr_{0.1}(Ga_{0.8}Fe_{0.2})_{0.8}Mg_{0.2}O_{3-\delta}$	1450	Cubic	300-1000	0.368
$La_{0.9}Sr_{0.1}(Ga_{0.7}Fe_{0.3})_{0.8}Mg_{0.2}O_{3-\delta}$	1450	Cubic	300-570	0.311
$La_{0.85}Sr_{0.1}(Ga_{0.9}Fe_{0.1})_{0.8}Mg_{0.2}O_{3-\delta}$	1450	Cubic	450-1000	0.578
$La_{0.9}Sr_{0.1}(Ga_{0.9}Co_{0.1})_{0.8}Mg_{0.2}O_{3-\delta}$	1450	Cubic	450-1000	0.707
$La_{0.9}Sr_{0.1}(Ga_{0.8}Co_{0.2})_{0.8}Mg_{0.2}O_{3-\delta}$	1450	Hexagonal	450-670	0.433
			670-1000	0.310
$La_{0.9}Sr_{0.1}(Ga_{0.75}Co_{0.25})_{0.8}Mg_{0.2}O_{3-\delta}$	1450	Hexagonal	100-450	0.231
			670-1000	0.192
$La_{0.9}Sr_{0.1}(Ga_{0.7}Co_{0.3})_{0.8}Mg_{0.2}O_{3-\delta}$	1450	Hexagonal	100-450	0.201
			500-780	0.265
$La_{0.85}Sr_{0.1}(Ga_{0.9}Co_{0.1})_{0.8}Mg_{0.2}O_{3-\delta}$	1450	Hexagonal	450-1000	0.694

From the results of Table 1 and Fig. 1, Fe was selected to be a dopant in LSGM and 0.2 mole of Sr was used in the base material. The selected compositions in the first year of this project were:

$La_{0.8}Sr_{0.2}Ga_{0.7}Mg_{0.3}O_{3-\delta}$ (LSGM)

$La_{0.8}Sr_{0.2}Ga_{0.7}Mg_{0.2}Fe_{0.1}O_{3-\delta}$ (LSGMF1)

$La_{0.8}Sr_{0.2}Ga_{0.7}Mg_{0.1}Fe_{0.2}O_{3-\delta}$ (LSGMF2)

$La_{0.8}Sr_{0.2}Ga_{0.7}Fe_{0.3}O_{3-\delta}$ (LSGF3)

The compositions were prepared by mixing La_2O_3, $SrCO_3$, Ga_2O_3, MgO and Fe_2O_3. Only La_2O_3 and MgO were calcined at 1000 °C to remove OH^- and $CO_3^=$ before weighing. Zirconia rods and absolute ethanol were used for the mixing of these oxide and carbonate materials. Although all reaction peaks detected by DTA ended before 1000 °C, the calcined temperature of 1250 °C was applied to all compositions of LSGM due to the remaining raw materials shown in XRD if firing below 1250 °C.

The calcined phases detected by XRD exhibited the other phases beside LSGM. The powder was recalcined if the other peaks still appeared in the XRD patterns. However, after sintering at 1500 °C with a soaking period for 2 hrs the single phase could be obtained in LSGM and LSGMF1 compositions from XRD with a resolution limit of diffractometer but not LSGF3 and LSGMF2. J. W. Stevenson et. al. [3] reported that the phase development of $(La_{0.9}Sr_{0.1})_xGa_{0.8}Mg_{0.2}O_{3-\delta}$ and $(La_{0.8}Sr_{0.2})_xGa_{0.8}Mg_{0.2}O_{3-\delta}$ could be different depending upon the firing temperature and the cations ratio between A-site and B-site as given in Table 2 and 3. The results from this reference showed the fraction of LSGM perovskite increased with increasing temperature and the cations ratio of 1. However, all compositions based on lanthanum gallate synthesized from this project were not reproducible, suggesting that LSGM compound was unstable. This was agreed with Prof. Brian Steele's opinion from Imperial College.

Because of a difficulty of reproducibility of LSGM and very expensive material of Ga_2O_3, the proposed alternative material was changed from the project title. LSGM based electrolyte materials was replaced by CeO_2.

$La_{1-x}Sr_xCo_{1-y}Fe_yO_{3-\delta}$ has been investigated as the cathode of SOFC. However, these compositions exhibited mixed electronic and ionic conductivity. Consequently, if the appropriate cations were doped and/or the amount of Co and Fe was altered in the proper way, the oxygen vacancies possibly increased and thus the ionic conductivity dominated. During the first year of this project, Sr and Gd were used to partially substituted into La-site as x=0.1 and 0.2 and the ratio of Co and Fe was adjusted to 0.3:0.7, 0.4:0.6 and 0.6:0.4.

The preparation of these base compositions was similar to LSGM. However, the mixed powder was calcined at 1100 °C with soaking at each reaction temperature determined from DTA. As shown in Fig. 2, the calcined phase of LSCF exhibited only one phase. After sintering at 1300 °C these compositions still remained a single phase. Also, the soaking times for 1 and 3 hrs insignificantly affected the density of these base compositions. However, the sintering temperature at 1450 °C with a soaking period for 2 hrs gave higher density and the other phase still could not be observed from XRD pattern as revealed in Fig. 2. The microstructure of sintered pellets after thermal etching in Figs. 3-4 was found that an increase of Fe dopant reduced the grain size. In addition, the intragranular pores could be observed in $La_{0.8}Sr_{0.2}Co_{0.6}Fe_{0.4}O_{3-\delta}$ as shown in Fig. 4. For the thermal expansion coefficient, the results showed a trend of increasing with amount of Co. In addition, the substrates appear to be blue around the sintered samples due to the chemical unstability of cobalt in the compositions. Therefore, the base electrolyte was changed to CeO_2 in the second year of this project.

Table 2. Phase development of $(La_{0.9}Sr_{0.1})_xGa_{0.8}Mg_{0.2}O_{3-\delta}$ [3]

Heat treatment in air	A/B cation ratio (x)				
	0.90	0.95	0.98	1.00	1.02
1200 °C 2 h	~93%Perovskite ~1%Tetragonal ~5%$SrLaGa_3O_7$ ~1%MgO	~92%Perovskite ~2%Tetragonal ~3%$SrLaGa_3O_7$ ~1%MgO ~2%$La_4Ga_2O_9$	~96%Perovskite ~2%Tetragonal ~1%$SrLaGa_3O_7$ ~1%MgO	~96%Perovskite ~3%Tetragonal ~1%MgO	~96%Perovskite ~4%$SrLaGaO_4$
1400 °C 2 h (1450 °C for x=1.02)	~95%Perovskite ~4%$SrLaGa_3O_7$ ~1%MgO	~99%Perovskite ~1%MgO	Perovskite	Perovskite	~99%Perovskite ~1%$SrLaGaO_4$
1500 °C 2 h	~95%Perovskite ~4%$SrLaGa_3O_7$ ~1%MgO	~99%Perovskite ~1%MgO	Perovskite	Perovskite	N/A
1500 °C 2 h	~94%Perovskite ~5%$SrLaGa_3O_7$ ~1%MgO	~99%Perovskite ~1%MgO	Perovskite	Perovskite	~99%Perovskite ~1%$SrLaGaO_4$

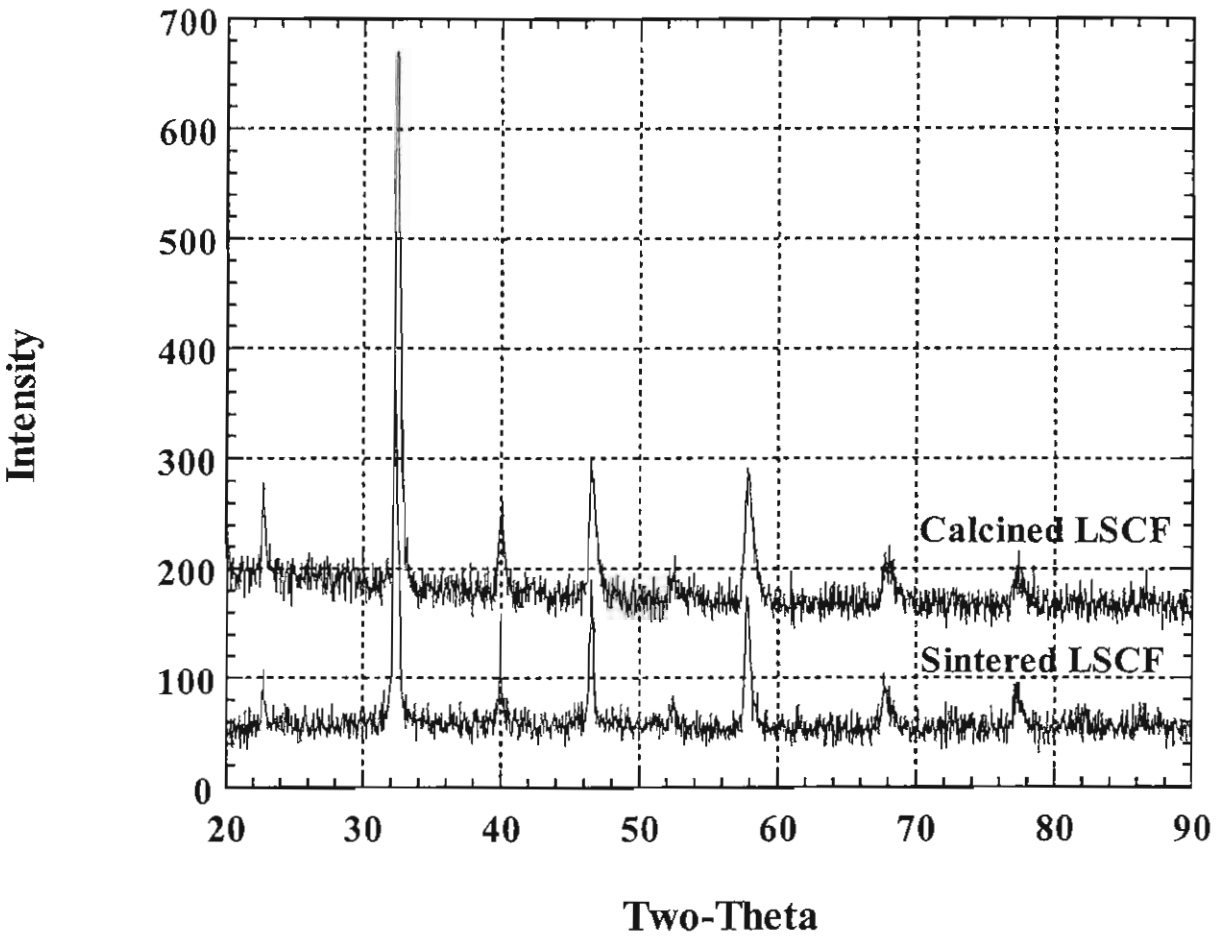

Fig. 2 XRD patterns of calcined powder and LSCF pellet after sintering at 1450 °C

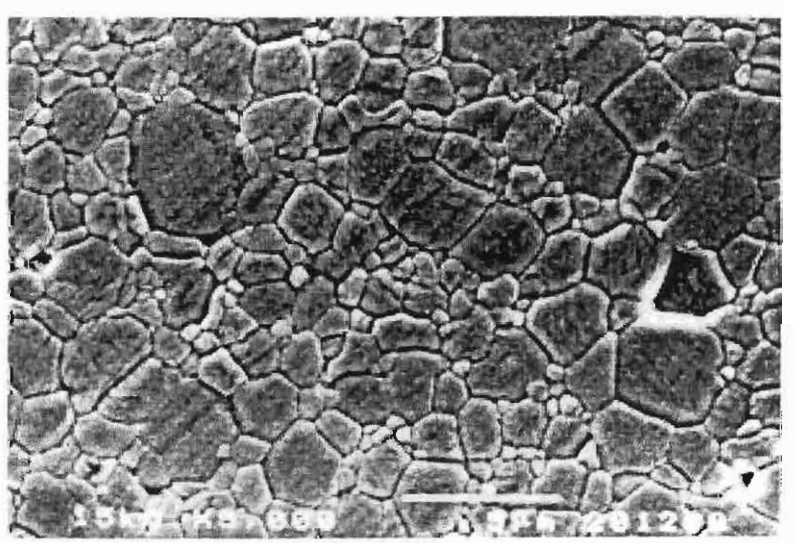

Fig. 3 SEM micrograph of $La_{0.8}Sr_{0.2}Co_{0.4}Fe_{0.6}O_{3-\delta}$ sintered at 1300 °C

Table 3. Phase development of $(La_{0.8}Sr_{0.2})_xGa_{0.8}Mg_{0.2}O_{3-\delta}$ [3]

Heat treatment in air	A/B cation ratio (x)		
	0.95	0.98	1.00
1200 °C 2 h	~70%Perovskite ~15%$SrLaGa_3O_7$ ~15%$SrLaGaO_4$	~70%Perovskite ~15%$SrLaGa_3O_7$ ~15%$SrLaGaO_4$	~72%Perovskite ~13%$SrLaGa_3O_7$ ~15%$SrLaGaO_4$
1400 °C 2 h	~89%Perovskite ~6%$SrLaGa_3O_7$ ~5%$SrLaGaO_4$	~91%Perovskite ~4%$SrLaGa_3O_7$ ~5%$SrLaGaO_4$	~91%Perovskite ~3%$SrLaGa_3O_7$ ~6%$SrLaGaO_4$
1500 °C 2 h	~96%Perovskite ~3%$SrLaGa_3O_7$ ~1%$SrLaGaO_4$	~99%Perovskite ~1%$SrLaGa_3O_7$	Perovskite

Ceria-based electrolytes show an ionic conductivity at 700 °C similar to ZrO_2 at 1000 °C [4], however they are not pure ionic conductors. In addition, ceria is not stable under the hydrogen environment.

Cerium [5] can exhibit both the +3 and +4 oxidation states and the oxide compositions in the range of Ce_2O_3 and CeO_2 can be formed. The final form is strongly dependent upon temperature and oxygen pressure. Pure CeO_2 is yellow in color and CeO_{2-x} is blue and turns almost black when it is grossly nonstoichiometric [6]. CeO_2 crystallizes in the fluorite structure, FCC unit cell with space group Fm3m (a=0.5411 nm from JCPDS 34-0394 in Appendix A) and is reduced at elevated temperatures and low oxygen pressures to form an oxygen deficient nonstoichiometric oxide. Defects in ceria can be either intrinsic attributing to thermal disorder and atmosphere or extrinsic formed by dopants. These defects affect the electrical conductivity of this material.

Ceria can be classified as a mixed conductor showing both electronic and ionic conduction. At high temperatures and low oxygen partial pressures, ceria behaves as an n-type semiconductor. Ionic conductivity resulting from the oxygen vacancies depends on the amount of dopants. It increases significantly when ceria is doped with aliovalent oxides such as CaO, Y_2O_3 and various rare earths. However, an increasing amount of dopants tends to form a second phase. G. B. Balaza and R.S. Glass reported that the

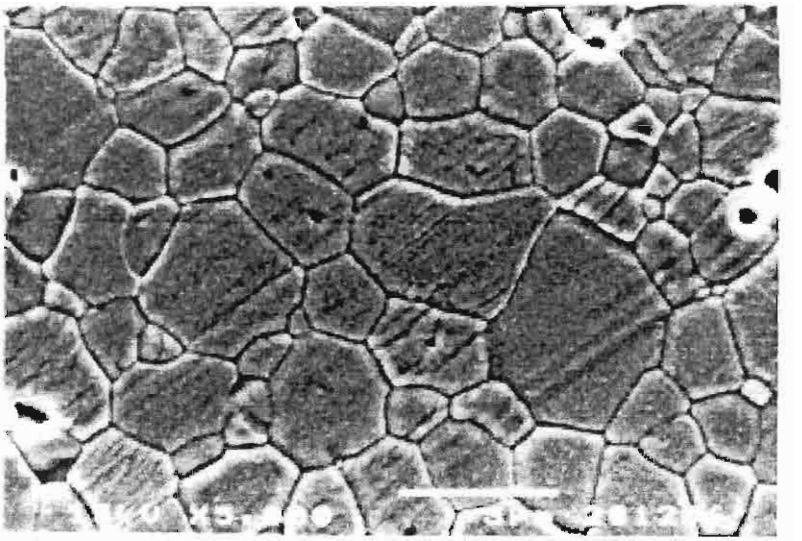

Fig. 4 SEM micrograph of $La_{0.8}Sr_{0.2}Co_{0.6}Fe_{0.4}O_{3-\delta}$ sintered at 1300 °C

Table 4: Evidence of second phase from x-ray spectrum for ceria doped with 10 mol% rare earth oxides in order of decreasing ionic radii. [7]

Rare earth dopant	Evidence of second phase in X-ray spectrum?
La_2O_3	Yes
Pr_2O_3	No
Nd_2O_3	Yes
Sm_2O_3	No
Eu_2O_3	Yes
Gd_2O_3	No
Tb_2O_3	No
Dy_2O_3	No
Ho_2O_3	No
Y_2O_3	No
Er_2O_3	No
Tm_2O_3	Yes
Yb_2O_3	Yes
Lu_2O_3	Yes
Sc_2O_3	Yes

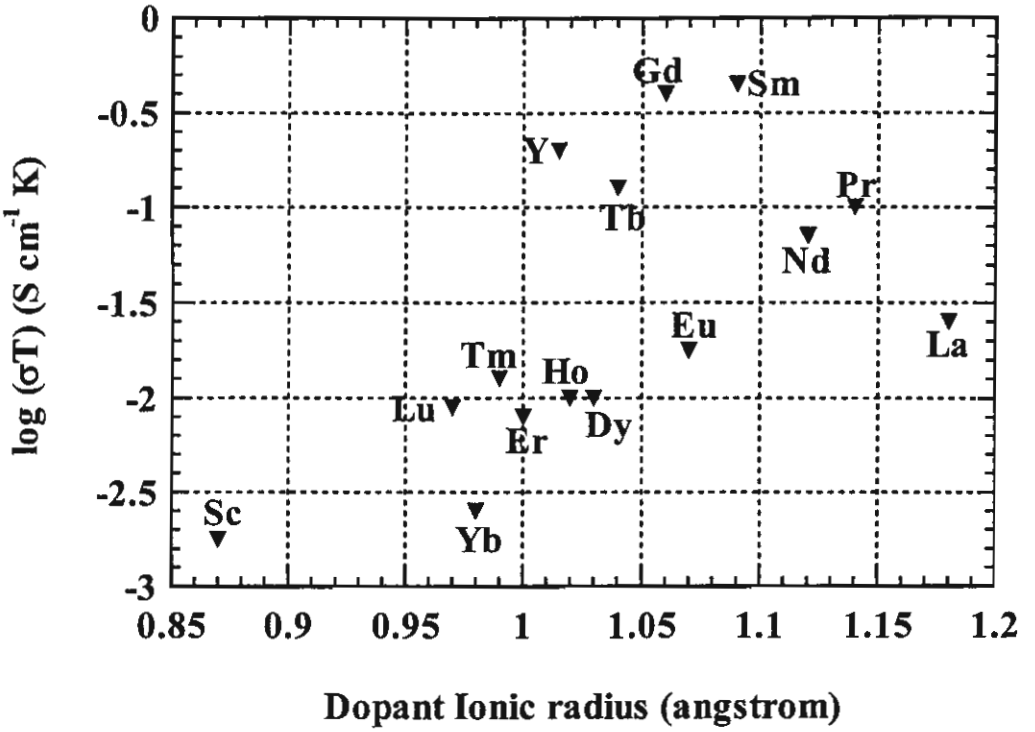

Fig. 5 Plot of conductivity of doped ceria at 400 °C versus ionic radius of rare earth cation [7]. Ionic radii taken from Ref. 9

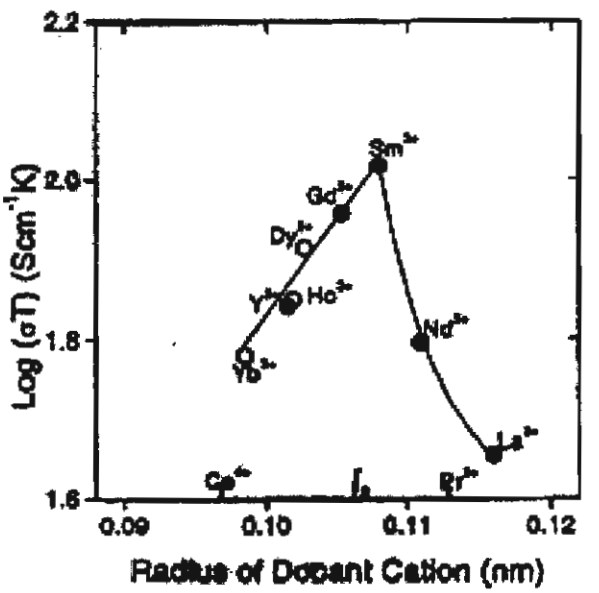

Fig. 6 Ionic conductivity of doped ceria at 800 °C vs the cation radius [8]

Table 5 Ionic conductivity data for selected electrolyte compositions [10].

Composition	Dopant	R_d (Å)	ΔE (eV)	σ, 500 °C ($S\ cm^{-1}$)	σ, 600 °C ($S\ cm^{-1}$)	σ, 700 °C ($S\ cm^{-1}$)
$Ce_{0.9}Gd_{0.1}O_{1.95}$	Gd^{3+}	1.053	0.64	0.0095	0.0253	0.0544
$Ce_{0.9}Sm_{0.1}O_{1.95}$	Sm^{3+}	1.079	0.66	0.0033	0.0090	0.0200
$Ce_{0.887}Y_{0.113}O_{1.9435}$	Y^{3+}	1.019	0.87	0.0087	0.0344	0.1015
$Ce_{0.8}Gd_{0.2}O_{1.9}$	Gd^{3+}	1.053	0.78	0.0053	0.0180	0.0470

addition of 10 mol% dopants did not appear to affect the sintering properties, with the exception of some rare earths as listed in Table 4 [7]. They also reported the conductivity as a function of ionic radius of dopant cation as shown in Fig. 5 [7]. From their results, Y, Sm and Gd exhibited the highest conductivities. In contrast, the ionic conductivity of doped ceria at 800 °C against the radius of dopants was reported by K. Eguchi et. al. [8] as shown in Fig. 6. From their work, Sm, Gd and Dy gave the high ionic conductivity. The values of ionic conductivity for those dopants were also given in Table 5 [10].

B.C.H Steele [10] suggested that the high conductivity was resulting form the low association enthalpy of $Re_{Ce}' - V_O^{\cdot\cdot}$ defect complexes. In addition, $Gd_{Ce}' - V_O^{\cdot\cdot}$ defect complexes were confirmed to exhibit the lowest binding energy [11]. B.C.H. Steele [10] summarized that the range of 9-11% $GdO_{1.5}$ should improve the performance of SOFC at 500 °C. Recently, T. Mori et. al. [12] have studied Sm, La and alkaline earth as co-dopant in CeO_2 and concluded that $(La_{0.75}Sr_{0.2}Ba_{0.05})_{0.175}Ce_{0.825}O_{1.83}$ gave high power density than $Ce_{0.8}Sm_{0.2}O_{1.9}$. Furthermore, the doubly doped ceria electrolyte with gadolinium and praseodymium [13] was reported to reduce the electronic conductivity and increase stability under hydrogen atmosphere.

In this project, the selection of dopants was based on not only the ionic radius of cations but also the electrical charge. The dopants with comparable size and lower charges (+3 and +2) would be used to add in CeO_2.

The second year works focused on the synthesized doped CeO_2, phase and microstructure after sintering, thermal expansion coefficient and conductivity. The

dopants were mostly selected from the rare-earth oxides. However, the main reason for a choice of cation depended on the lower charge, comparable size to cerium ion and the cost of materials. The cations selected for this research were indicated in Table 6. The specified ionic radii shown in Table 6 were from Ref. [14] and Ref. [9]. However, both values were different.

Only single cation doped ceria but different amount was investigated in this project. All doped ceria compositions were prepared by mixing all raw oxide materials (Appendix B) with zirconia balls and absolute ethanol in a polypropylene bottle. After drying and calcining at 1000-1200 °C depending on the dopants, the milled calcined powder was pressed into pellets and bars with a uniaxial hydraulic press and followed by cold isostatic press of 250-285 MPa. All doped compositions were sintered at 1450-1500 °C with the soaking time for 2, 5 and 10 hrs. Exceptionally, Bi-doped ceria was sintered at 1100 and 1250 °C with a soaking period of 1 hr. Sintering at higher temperature yielded the bloated pellets and bars.

Table 6: Valence, Ionic Radii and the amount of selected cation dopants used in this work

Ion	Valence	Radius (Å)[14]	Radius (Å)[9]	maximum mol% used in this project
Bi	+3	0.93		10
Ce	+4	0.97	0.97	based composition
Ce	+3		1.04	
Dy	+3	0.92	1.03	30
Er	+3	0.97	1.00	20
Gd	+3	1.04	1.05	30
Sm	+3	1.00	1.08	10
Sn	+2	0.93		10
Y	+3	0.95	1.02	20

The phases of calcined powder and sintered pellets were detected by XRD (Jeol, JDX3530). The results* found the extra peaks for 30 mol% Dy-, 20 mol% Er- and 10 mol% Sn-doped ceria after calcination. After sintering at 1500 °C, the single phase still existed for all doped compositions except 10 mol% Sn dopant determined from the small peaks of two-theta at 26.6, 33.9 and 51.8.

The effects of dopants and their amount on the grain size, shape and porosity of ceria could be observed from SEM micrographs*. Increasing amount of Gd and Dy tended to increase the grain size. In contrast, Y and Sn decreased the grain size. Although an increase of Sn amount yielded higher porosity, the second try got the opposite result from the previous one. For Er dopant, the bimodal grain sizes could be observed as an amount of Er increased.

The results of thermal expansion coefficient (TEC) for some sintered doped CeO_2 indicated that Gd and Sn reduced the TEC of CeO_2 but Y increased it. Up to 10 mol% Bi unaffected TEC.

The last year of this project would concentrate on the electrical conductivities for the selected compositions. Both DC-4 point and ac impedance measurements for some cations doped ceria would be collected in air, oxygen (99.5%) and carbon monoxide (99.3%) to investigate the stability in both oxidizing and reducing atmospheres. In addition, the comparison of conductivity before and after heat treatment at 700 °C for 90 hrs with flowing oxygen would be examined and their microstructure would be investigated by SEM.

AC Impedance measurement

Impedance measurements are used to study the properties of solid electrolytes related to [15]:

a. Transport number, concentrations of charge carriers, electronic and ionic defects and their mobility.

---

* Fig. shown in the second year annual report

b. Effect on conductivity of oxygen partial pressure, dopant concentration, impurities, grain boundaries and second phase precipitation.
c. Charge-transfer and polarization phenomena at the electrolyte-electrode interface (noble metals are often chosen for electrodes as they are assumed to be chemically inert)

In ceramics, ac impedance can be used to resolve the resistance due to grain interiors and the grain boundaries [16]. This has facilitated the study of some processes such as sintering, grain growth and solid state precipitation. The technique is useful for zirconia ceramics.

Bulk properties such as conductivity are calculated using the length over area (l/A) of each sample. For measurement of grain interior or grain boundary properties [16], surface finish is not critical, as this only affects the electrode impedance. If the grain boundary and electrode arcs partly overlap, the resolution can sometimes be improved by polishing.

Electrodes are usually made of the precious metals such as silver, platinum, gold or graphite and normally applied to the samples by painting, vacuum evaporation or sputtering. The samples should be fired at 500-600 °C to remove traces of organic compounds from the electrode. The electrode characteristics of gold and platinum are similar in the temperature range up to 500 °C, relatively blocking to oxygen but silver gives a lower electrode impedance [16]. For this project, gold is used as electrode due to very expensive platinum and evaporation of silver after measurement at high temperature for a long time.

Experimental Procedure

The dc conductivity of sintered bars was measured as a function of temperature. Fired-on gold electrode was applied on the samples before measurement. The data were collected from 150 °C to 800 °C with a heating rate of 4 °C /min. Below 230 °C the data were scattering due to high resistance.

The ac impedance of sintered pellet was determined from Solartron SI1260. Fired-on gold electrode was applied on both sides of pellet and fired at 840 °C before measurement. The data were collected in air every 50 °C from 300 °C to 600 °C or 700 °C for some samples and in oxygen from 500-650 °C. At each temperature measurement, the frequency range swept from 10^7 Hz to 0.1 Hz. The amplitude of the ac signal imposed on the sample was 30 mV as followed from the instrument manual. The thermocouple was placed close to the sample. Both thermocouple and sample were on the sample holder inside the tube furnace.

After ac impedance measurement, the selected samples were heated at 700 °C in the tube furnace with flowing oxygen for 90 hrs and then the impedance measurements were repeated between 500 °C to 600 °C by Solartron with the same setup of instrument as used before. The measurements were carried out in air and carbon monoxide. The Zplot program [17] was used to display the results of Z' and Z'' measurements.

The heat-treated samples were polished down to 1 micron with diamond paste and thermally etched at 75 °C below the sintering temperature with a soaking time for 2 hrs before gold sputtering. The microstructure of the specimens was observed by scanning electron microscope (Jeol, JSM5410).

Results and Discussion

Figs 7-10 show the Arrhenius plots of dc-conductivity of cations doped-ceria. Fig. 7 gives the results of 20 and 30 mol% Dy-doped ceria. As the amount of Dy increases, the dc conductivity of ceria increases. In addition, 30 mol% Dy exhibit a stable conductivity in a wide range of temperatures. The measurement conductance as a function of increasing temperature is not continuous. This might be possibly due to either a loose connection or its transition temperature of Dy-doped ceria. Although the retest has not been done, the measurement conductance during cooling gives the same result but lower values. For Gd dopant, 15 mol% give higher conductivity than 20 mol% in the temperature above 475 °C as illustrated in Fig. 8. Fig. 9 represents the result of conductivity for 5 and 20 mol% Y-doped ceria. Its values increase with the amount of Y. In general, the number of oxygen vacancies are attributable to the amount of dopants. However, the conductivity values of Gd- and Y-doped ceria from this project are lower than those from other works [7, 18]. The comparison of conductivity for selected dopants in ceria is indicated in Fig. 10. The results show that 20 mol% Er-doped ceria give higher

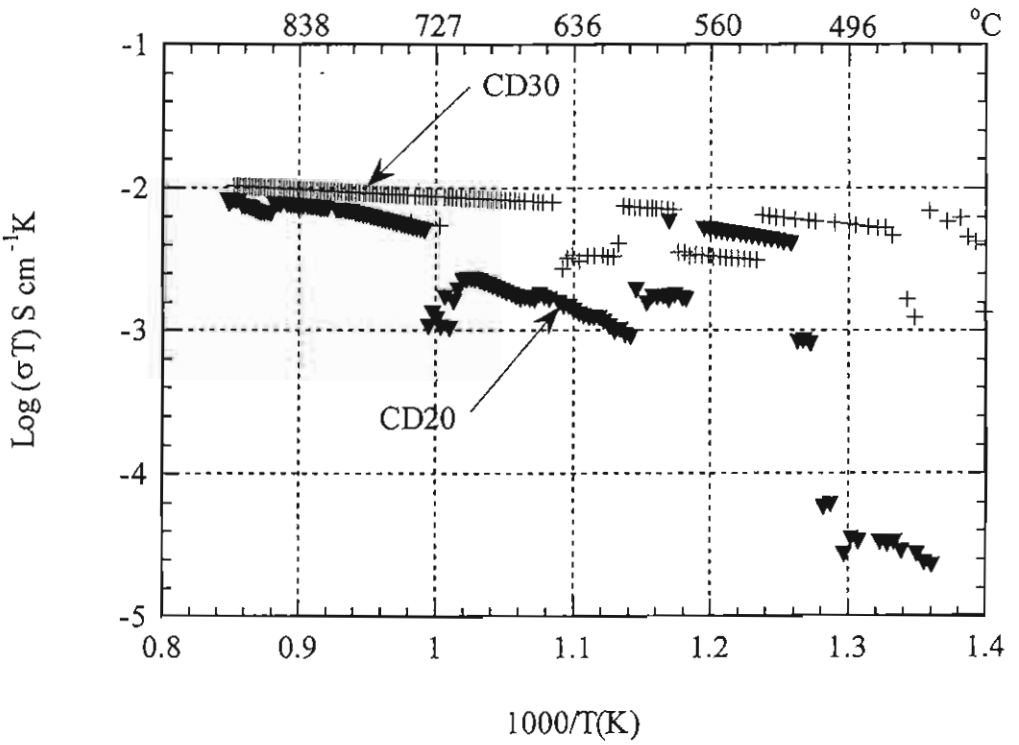

Fig. 7 DC conductivity vs. reciprocal temperature of Dy-doped ceria

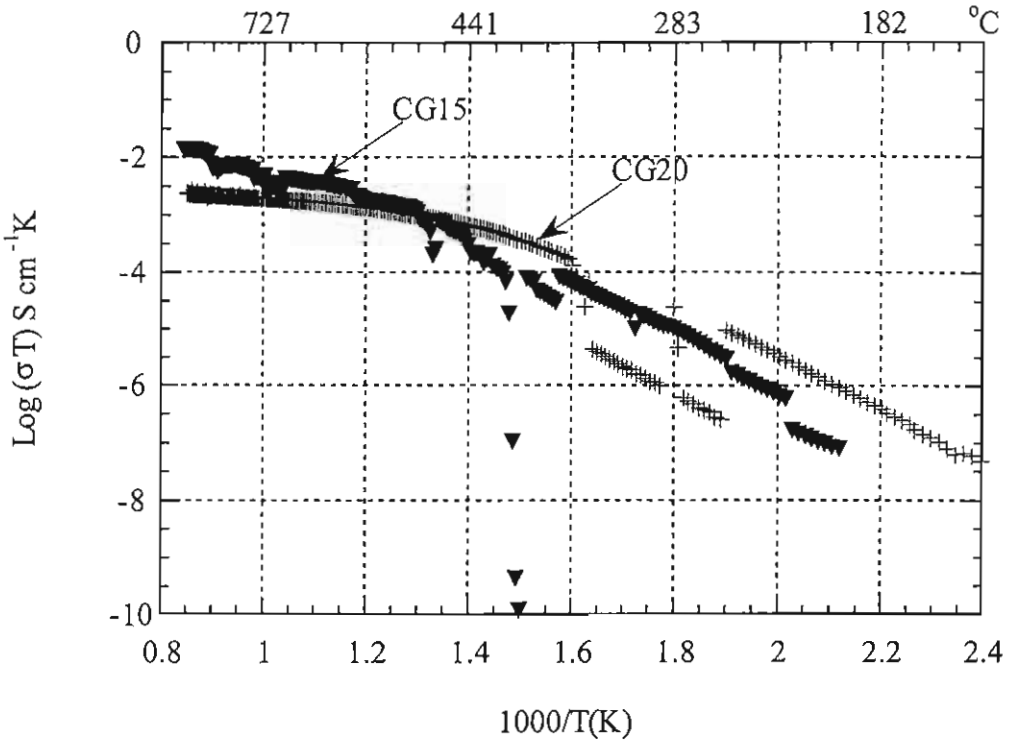

Fig. 8 DC conductivity vs. reciprocal temperature of Gd-doped ceria

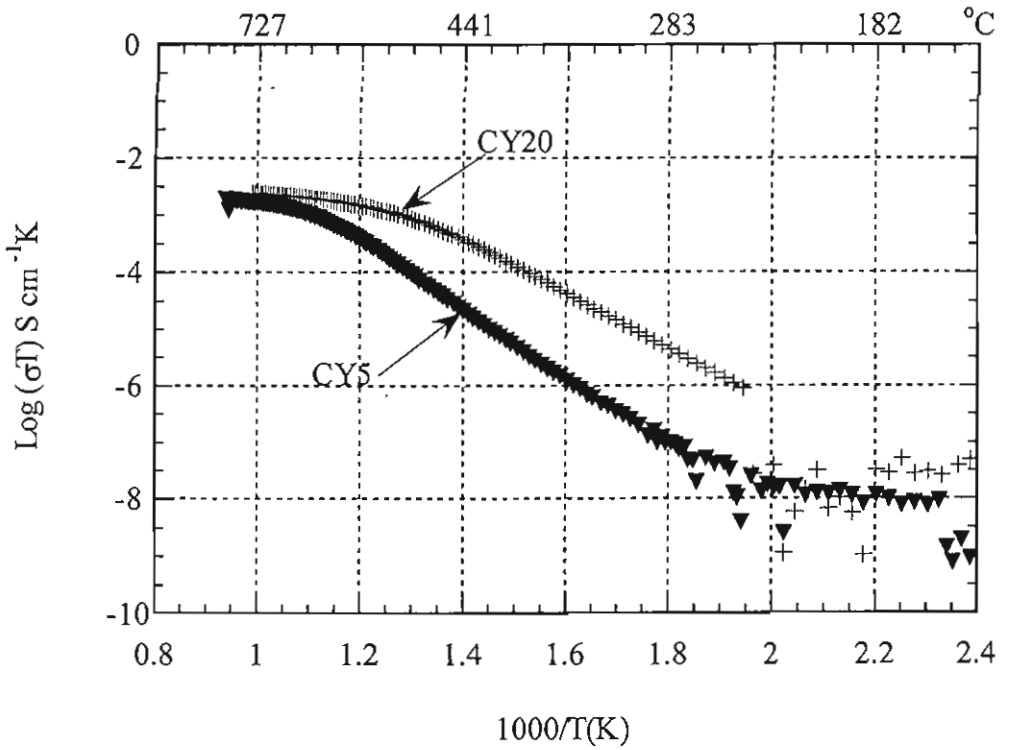

Fig. 9 DC conductivity vs. reciprocal temperature of Y-doped ceria

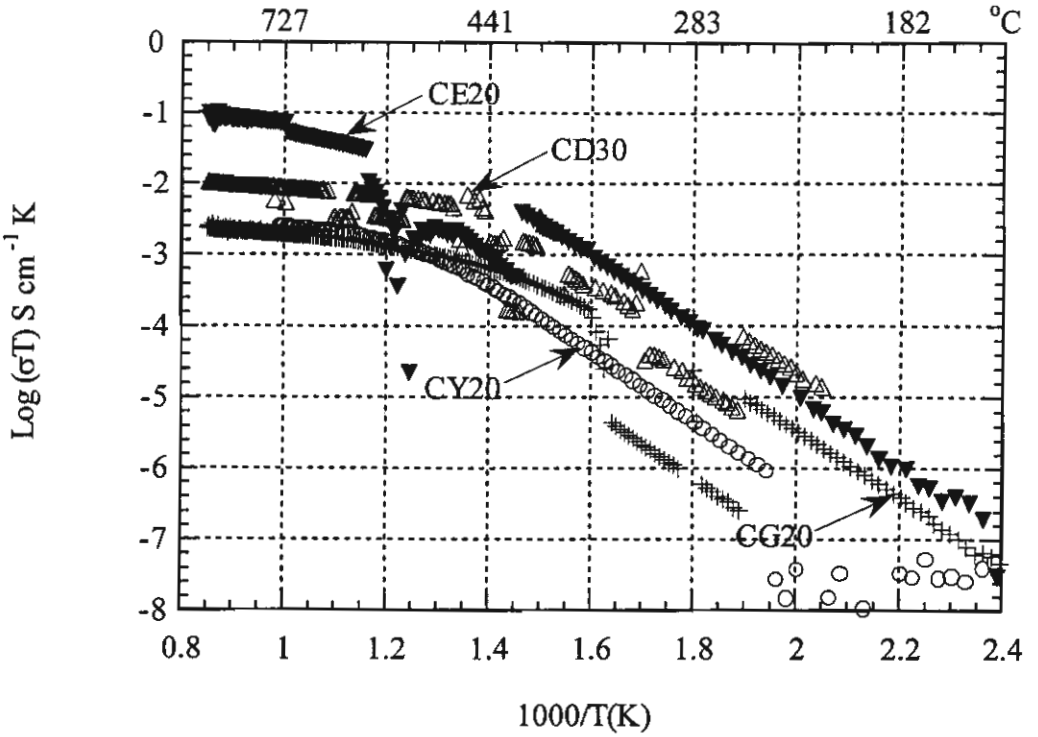

Fig. 10 DC conductivity vs. reciprocal temperature of selected cation dopants

dc conductivity than 30 mol% Dy, 20 mol% Gd and 20 mol% Y. Nevertheless, the more stability of conductivity above 500 °C can be obtained from 30 mol% Dy-dopant.

Figs. 11-13 represent the impedance spectra of 30 mol% Gd-doped ceria measurement in air at different temperatures. Figs. 14-15 also show the same trend of impedance spectra for 10 mol% Sm-doped ceria measured in air at 550-700 °C and Fig. 16 for 20 mol% Y in ceria at 600 and 650 °C. The results of all compositions in this work show the higher temperature the lower magnitude of impedance, both of real and imaginary parts. This implies that the conductivity of doped ceria can be achieved at higher temperature. The impedance spectra are associated with the bulk crystal lattice and with the grain boundary [16]. This is critical because the overall ionic conductivity is composed of the sum of these impedances and the effect of temperature on the relative contributions of each process makes it complicated. In addition, Wang and Novick [19] reported the presence of high resistivity material along the grain boundaries caused an extra arc in the impedance spectra. The effect also was greatest for dilute solid solutions and almost disappeared for dopant concentration greater than 15 mol%. Their work used

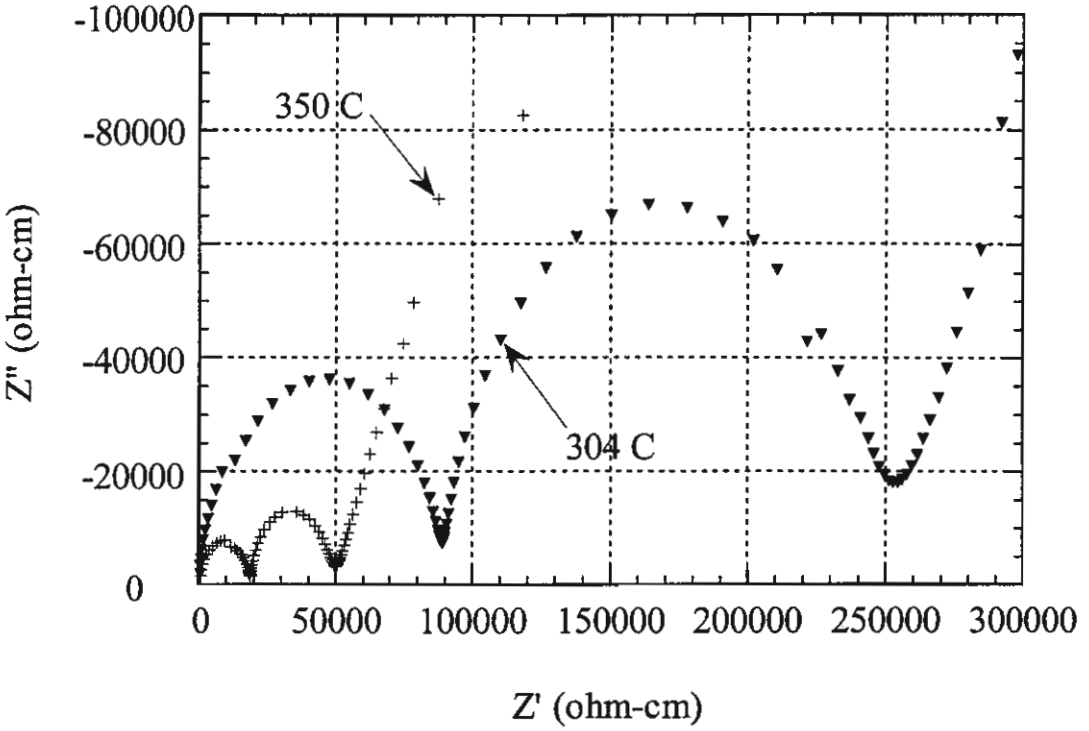

Fig. 11 Impedance spectra for $Ce_{0.7}Gd_{0.3}O_{2-x}$ measurement at 304 and 350 °C

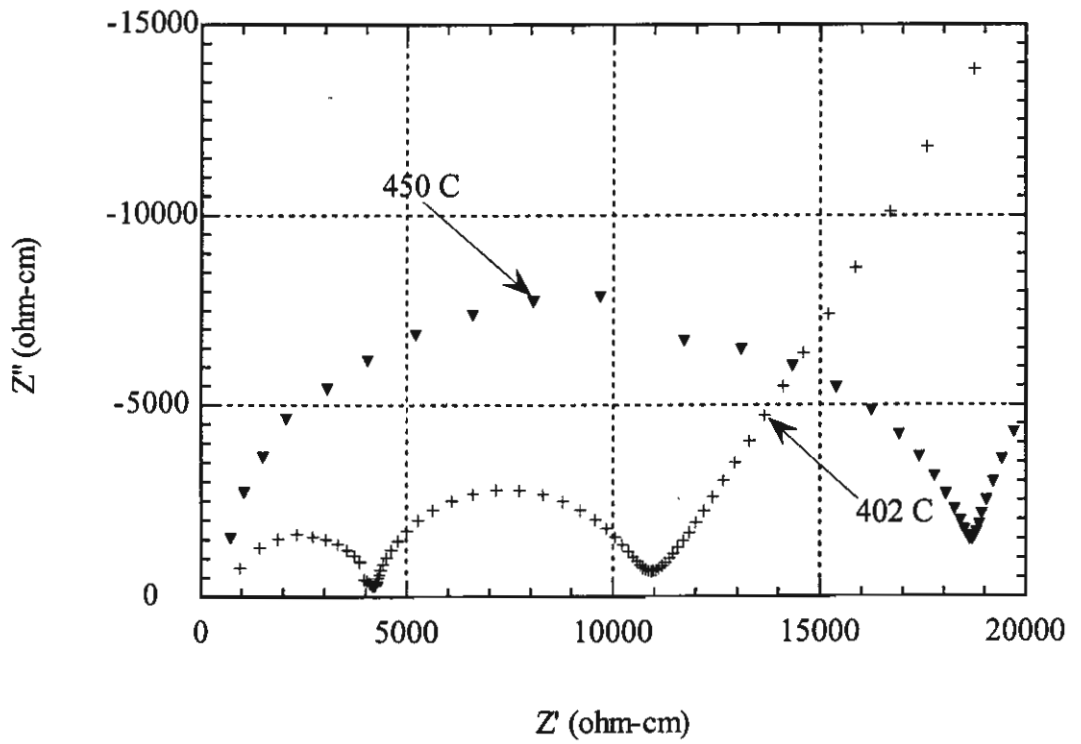

Fig. 12 Impedance spectra for $Ce_{0.7}Gd_{0.3}O_{2-x}$ measurement at 402 and 450 °C

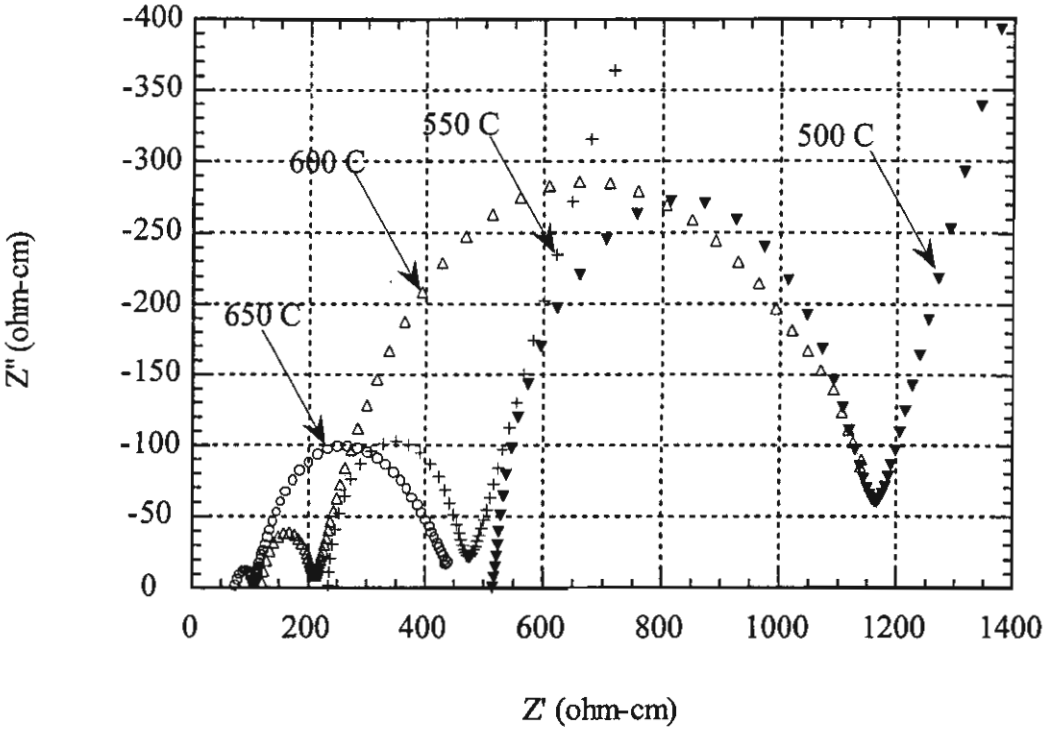

Fig. 13 Impedance spectra for $Ce_{0.7}Gd_{0.3}O_{2-x}$ measurement at 500 to 650 °C

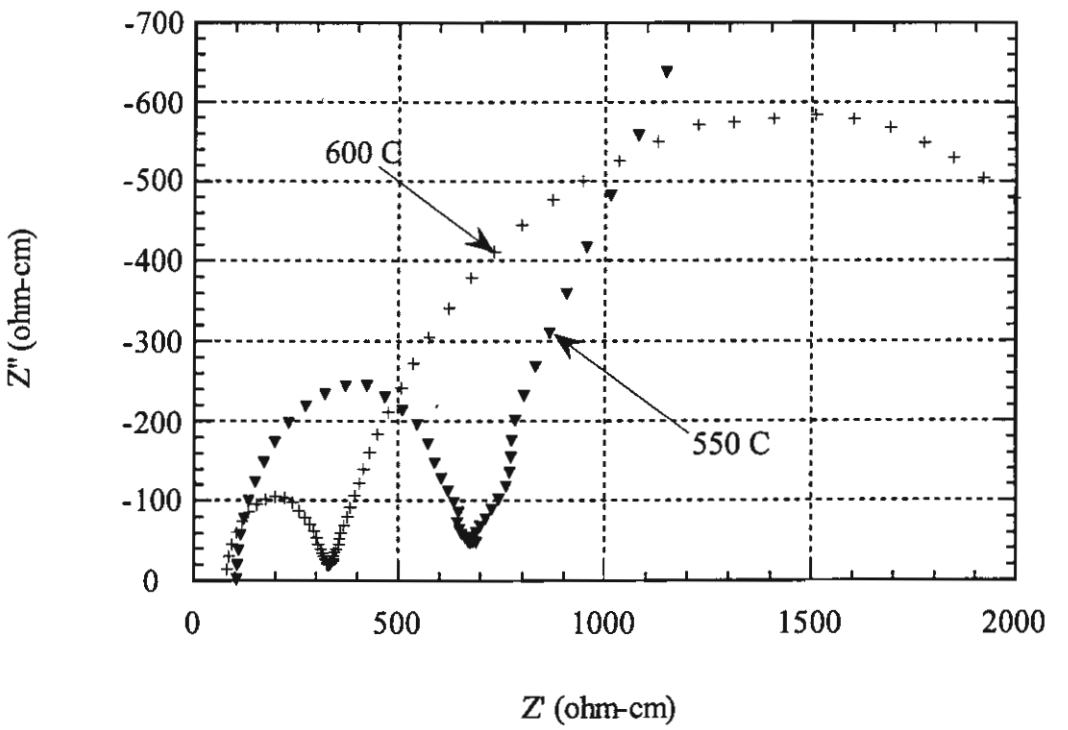

Fig. 14 Impedance spectra for $Ce_{0.9}Sm_{0.1}O_{2-x}$ measurement at 550 and 600 °C

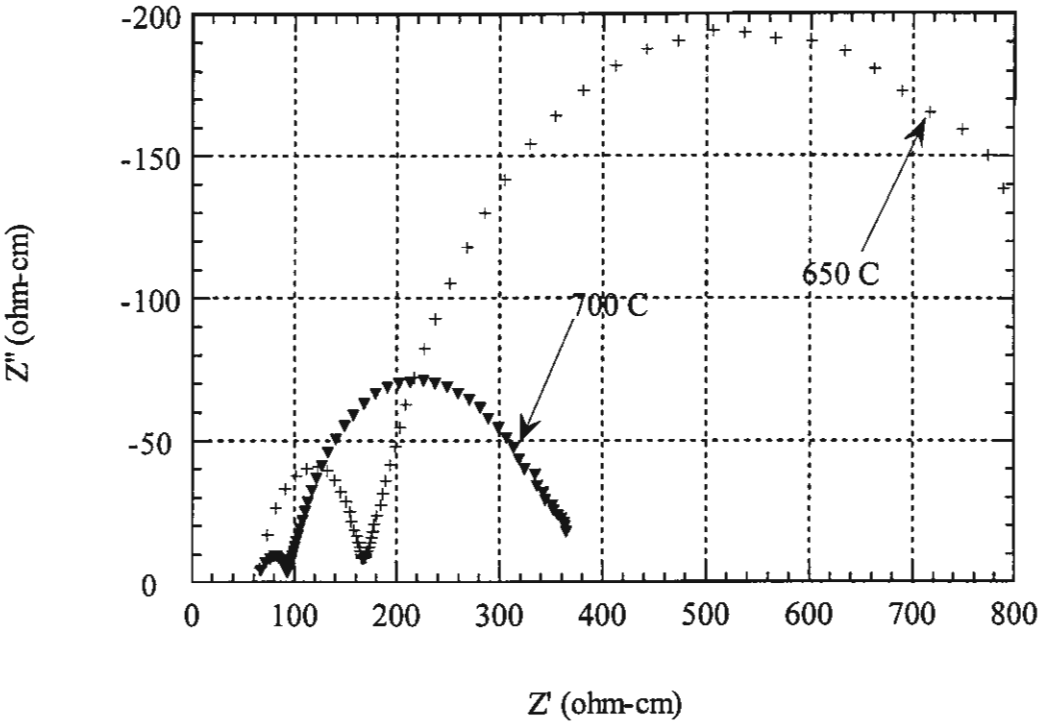

Fig. 15 Impedance spectra for $Ce_{0.9}Sm_{0.1}O_{2-x}$ measurement at 650 and 700 °C

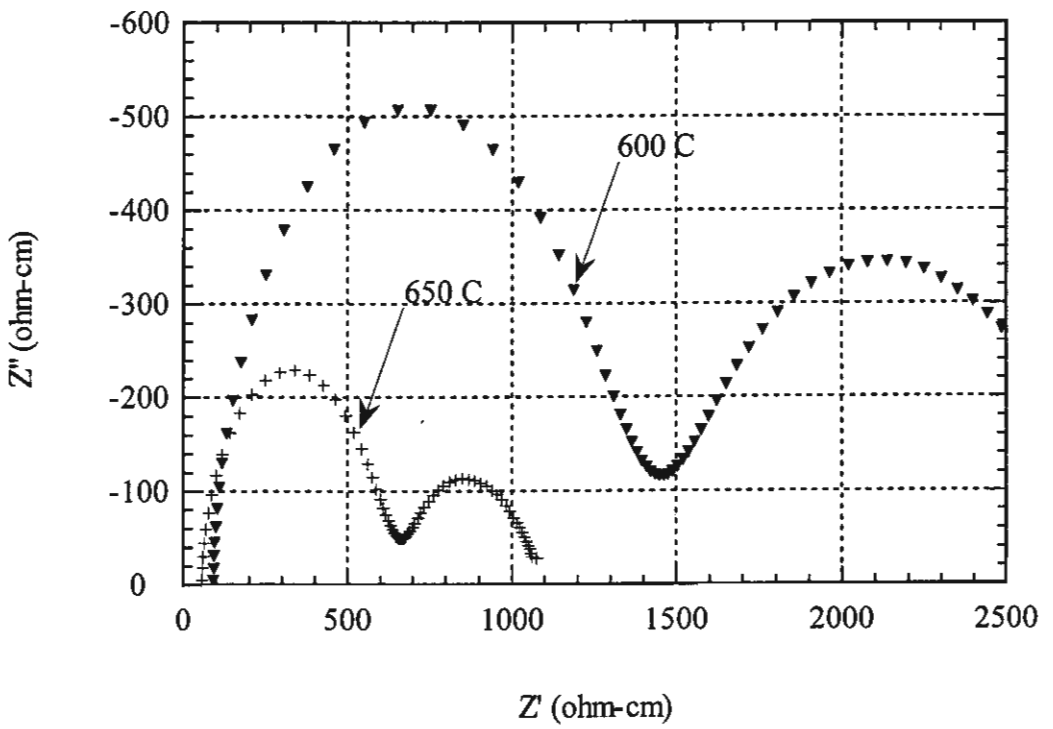

Fig. 16 Impedance spectra for $Ce_{0.8}Y_{0.2}O_{2-x}$ measurement at 600 and 650 °C

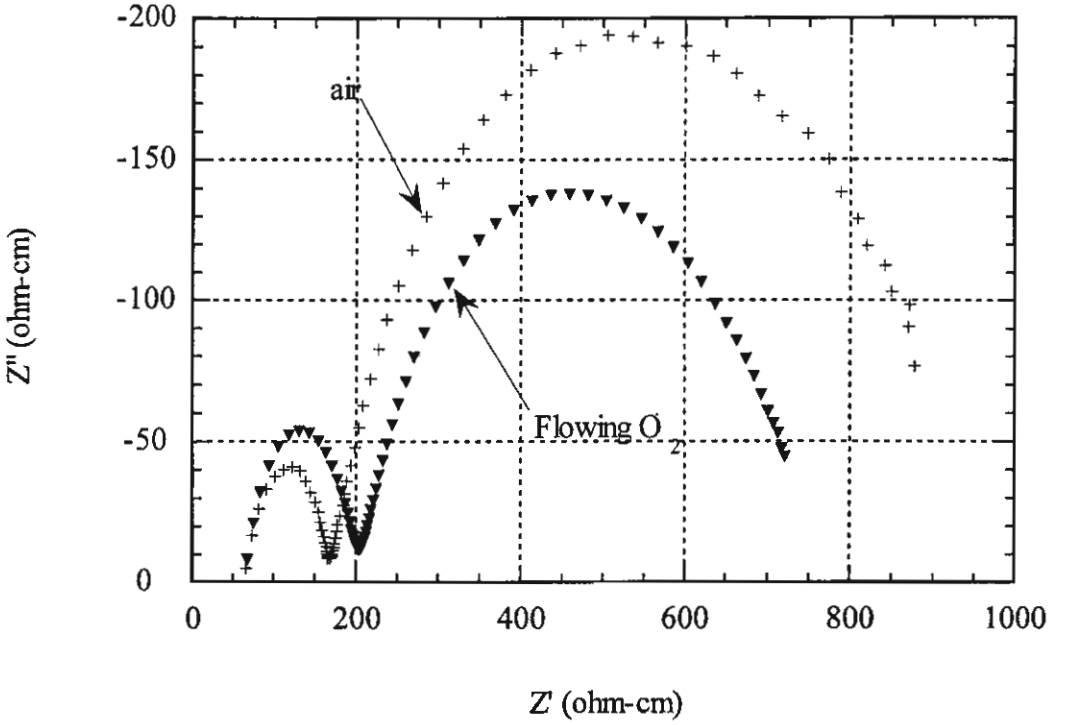

Fig. 17 Impedance spectra for $Ce_{0.9}Sm_{0.1}O_{2-x}$ measurement in air and O_2 at 650 °C

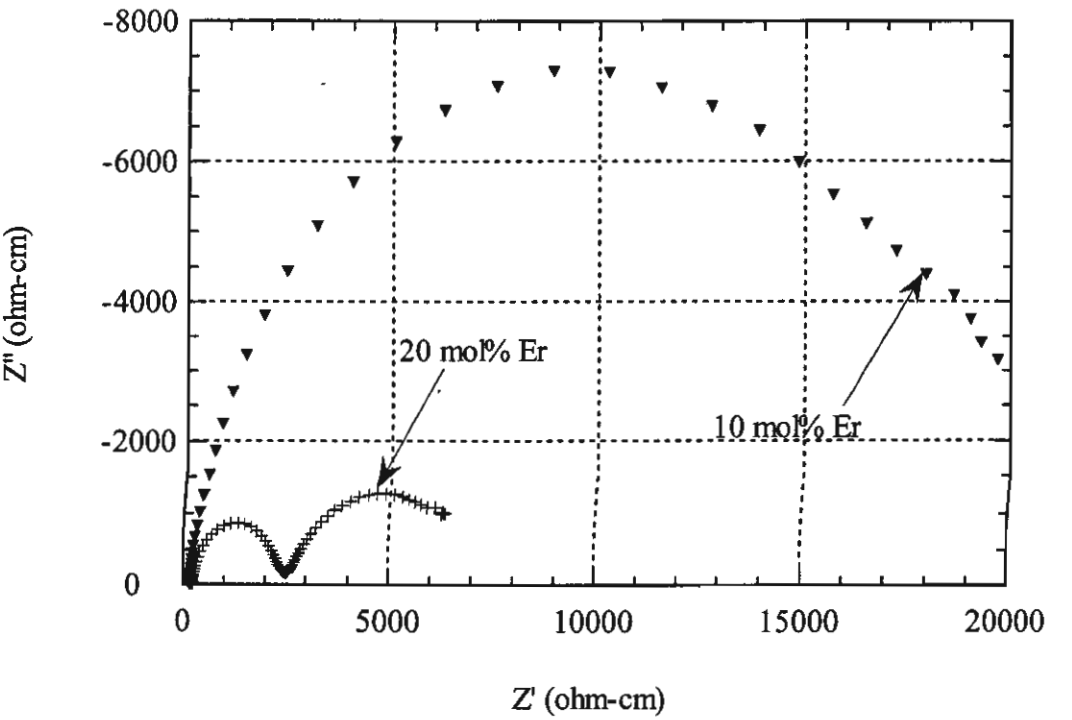

Fig. 18 Impedance spectra for 10 and 20 mol% Er-doped CeO_2 measurement at 550 °C

Y- and Ca- as dopants in ceria. No further work to investigate the composition along grain boundary is made in this project due to time consuming for sample preparation of Transmission electron microscopy (TEM).

Fig. 17 illustrates the effect of oxygen on the impedance of 10 mol% Sm-doped ceria at 650 °C as compared to that carried out in air. The less difference between the first and second arc of impedance can be observed in oxygen, suggesting that oxygen partial pressure affects the conductivity of doped ceria compositions, probably occurring at grain boundary.

The amount of dopants also influences the ionic conductivity of materials. As appeared in Fig. 18, the impedance of 20 mol% Er- is less than that of 10 mol% Er-doped ceria at measurement temperature of 550 °C. These also occur at the other measurement temperatures. The same results also obtained with Dy-doped ceria as observed in Fig. 19. 30 mol% Dy show lower impedance than 10 mol% Dy. These results imply that increasing amount of dopant can improve the conductivity of ceria unless the second phase does exist.

Fig. 20 presents the effect of soaking time at sintering temperature of 10 mol% Dy-dope ceria. 5 hrs soaking period can provide the less impedance than that of 2 hrs. In addition, the difference of interception on Z' axis between the first and second arc is much less than in the sample with a soaking time for 5 hrs. In general, the impedance inside grain is lower than that at grain boundary and also longer soaking time at sintering temperature performs larger grains and less grain boundaries. This can be seen from SEM photomicrographs in Figs. 38 and 39, respectively.

Figs. 21 and 22 illustrate the impedance spectra of some selected dopants in ceria measured in air at 500 °C and in oxygen at 600 °C, respectively. From the results, 30 mol% Gd give the lowest impedance than the other dopants. The order from the lowest to the highest impedance obtained from these results is 30 mol% Gd, 30 mol% Dy, 10 mol% Sm, 20 mol% Er and 20 mol% Y, respectively. All of them present the grain boundary resistance higher than bulk resistance. As temperature decreases, the

resistances of grain boundary and bulk are significantly different. As compared with the different dopants but the same amount, Figs. 23-25 represent the effect of 10 mol% for different dopants on the impedance spectra. Sm gives the lowest impedance as compared to Dy and Gd as observed in Figs. 23-24. Fig. 25 shows that Dy-doped ceria offers the lower impedance than Er dopant. Consequently, the effective dopants to lower the impedance of ceria order from the most efficient one, Sm > Gd > Dy > Er >Y.

Figs 26-28 show the impedance spectra before and after heat treatment at 700 °C for 90 hrs of 20 mol% Er-, 30 mol% Gd- and 20 mol% Y-doped ceria. The results indicate that the grain boundary resistance increases after heat treatment. This effect on 20 mol% Y is less than the other dopant. This might be due to alteration of composition at the grain boundary. Although the expected operating temperature should be lower than 700 °C, this temperature is desired to expedite the effect of longer period of operation.

Figs. 29-32 display the effect of carbon monoxide (CO) on the impedance of ceria for 30 mol% Dy at 500 °C, 30 mol% Gd at 550 °C, 10 mol% Sm at 550 °C and 20 mol% Y at 500 °C, respectively. These results imply that doped ceria compositions are not stable on CO atmosphere. Measurement at higher temperature than 550 °C, either explosion or autoignition occurs and impedance measurement has been stopped.

SEM photomicrographs of polished samples after heat treatment at 700 °C in oxygen for 90 hrs can be observed in Figs. 33-40. The difference of grain size and shape before and after heat treatment cannot be detected. As mentioned earlier, this might occur at the grain boundary and only TEM, a very high magnification microscope, possibly reveals this change. Figs. 37 and 38 show the etching pitch on the grain and at the grain boundary of 30 mol% Gd- and 10 mol% Sm-doped ceria, suggesting that soaking time for thermal etching temperature might take too long.

Summary and Conclusions

This project aims to improve the electrical properties by cation dopants into electrolyte materials of solid oxide fuel cell to lower the operating temperatures. $La_{1-x}Sr_xGa_{1-y}Mg_yO_{3-\delta}$ (LSGM), $La_{1-}Sr_xCo_{1-y}Fe_yO_{3-\delta}$ (LSCF) and CeO_2 are used as base materials in this research. The experimental investigation concentrates on the optimum dopants to obtain the single phase, well-defined microstructure and electrical conductivity in oxidizing and reducing atmospheres at different temperatures. In addition, the stability after operating for 90 hrs at 700 °C is examined. The cation dopants are selected from the rare-earth oxides having lower charge and comparable size to the substituted base materials.

The phases of LSGM and doped LSGM are found with the other unidentified phases detected by XRD in both calcined and sintered materials. Although firing at higher temperature and/or firing more than once can remove the second phase, the extra effort and careful is required to reproduce these based and doped compositions. In addition, Ga_2O_3 is expensive and time consuming to receive after ordering.

The single phase of LSCF can be achieved without difficulty. However, cobalt diffuses from the composition to deposit in the substrate and makes it impossible to control the amount of cobalt in the compound. Moreover, the thermal expansion coefficient increases with the amount of cobalt.

For cations doped ceria electrolyte, most rare-earth oxides can be doped into ceria with the amount up to 30 mol% without the second phase determined form XRD with a resolution limit of equipment.

For SEM photomicrographs, an increasing amount of Gd, Dy and Er increases the grain size of ceria. In contrast, an increasing amount of Y and Sn decreases the grain size. The longer soaking time at sintering temperature also affects the larger grain size.

For impedance measurement, an increasing amount of rare-earth dopant reduces the impedance of compositions, resulting the higher conductivity. This effect occurs to

all dopants in this investigation. However, as compared to all rare-earth dopants used in this project, Sm is the most effective dopant to achieve the lowest impedance. Furthermore, the oxidizing atmosphere during measurement gives the better conductivity in the term of lowering difference between the impedance of grain and grain boundary. The stability of doped-ceria is not probably suitable in carbon monoxide atmosphere and after longer period of operating. However, more experiments should be made and tested to confirm this result.

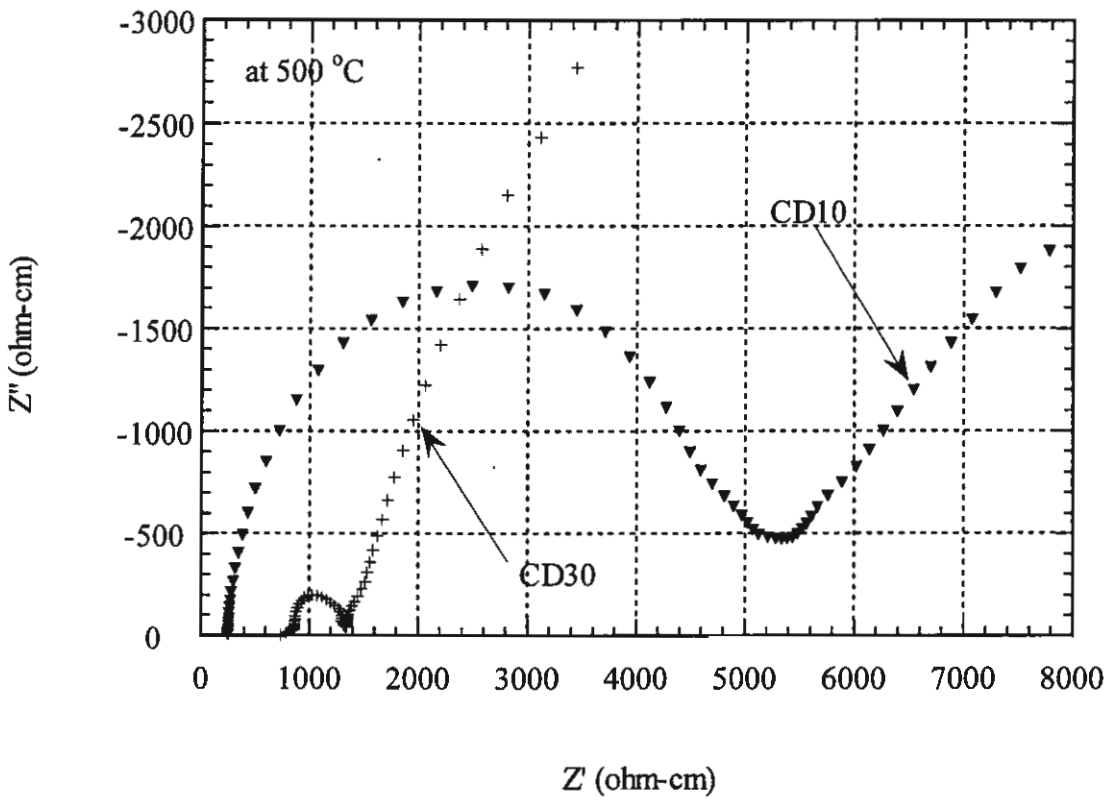

Fig. 19 Impedance spectra for 10 and 30 mol% Dy-doped CeO_2 measurement at 500 °C

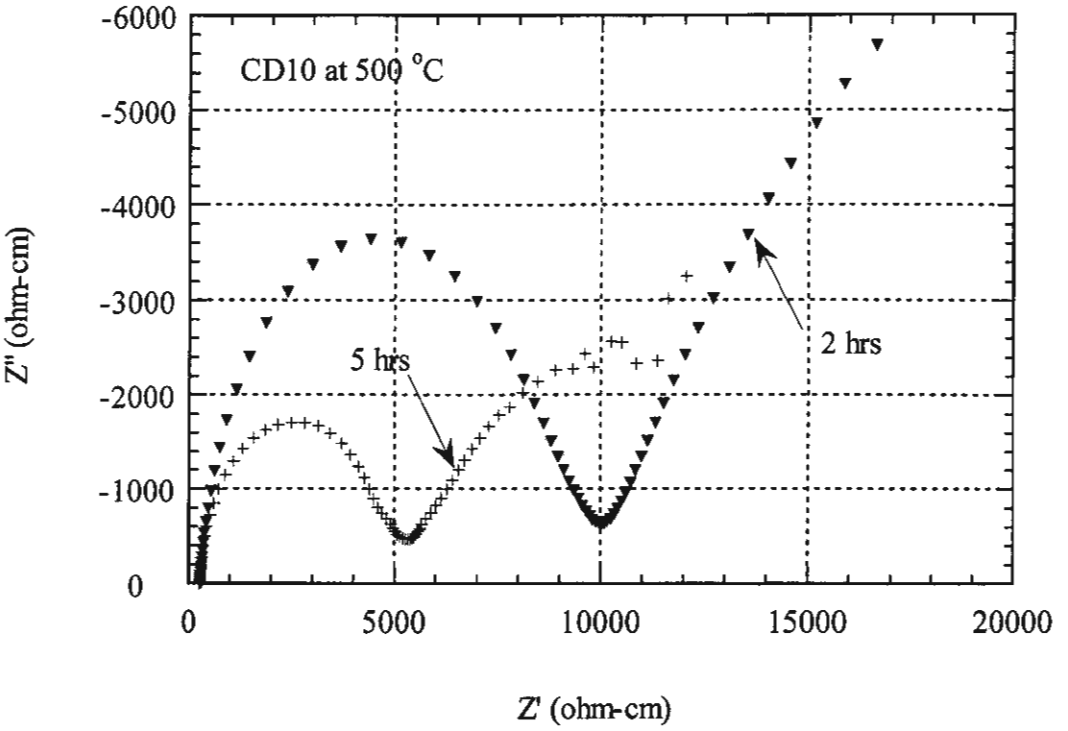

Fig. 20 Impedance spectra for 10 mol% Dy-doped CeO_2 with different soaking time

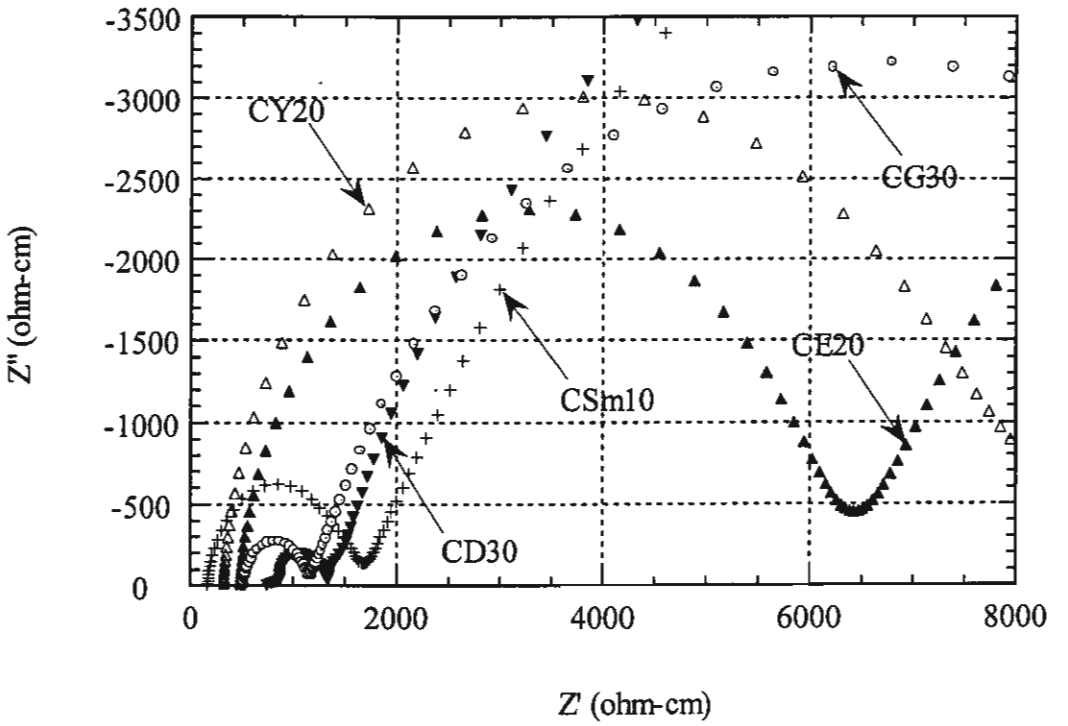

Fig. 21 Impedance spectra for selected cations doped CeO_2 measurement at 500 °C

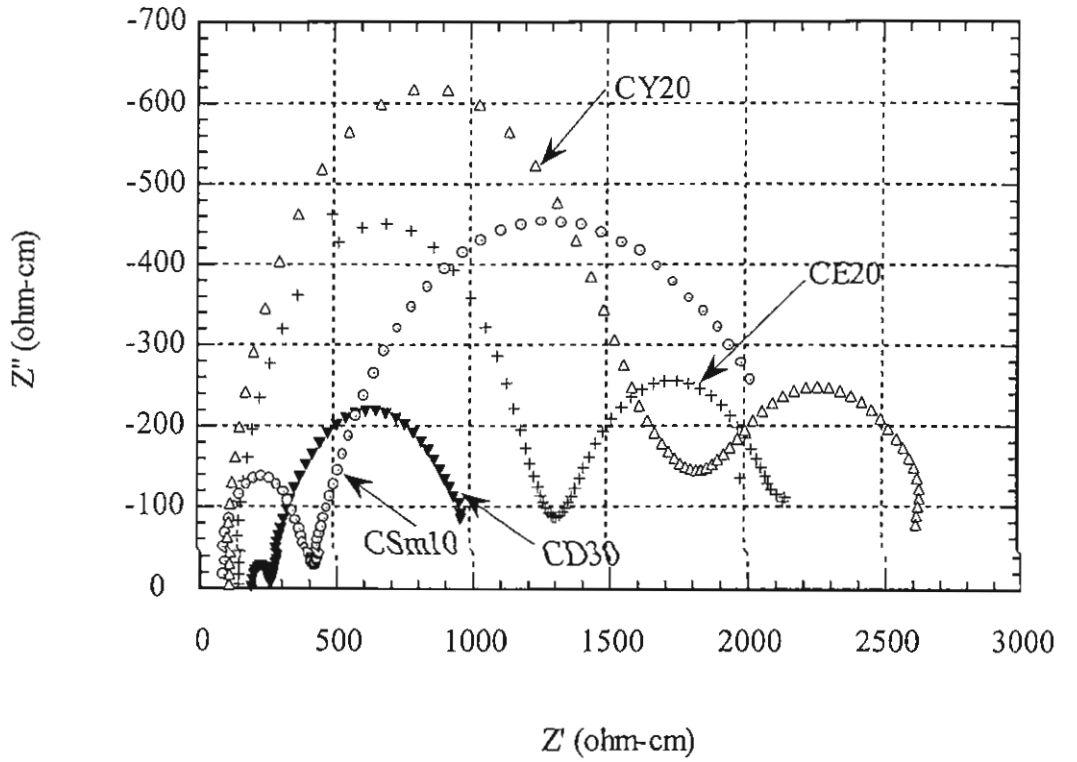

Fig. 22 Impedance spectra for selected doped CeO_2 measurement in O_2 at 600 °C

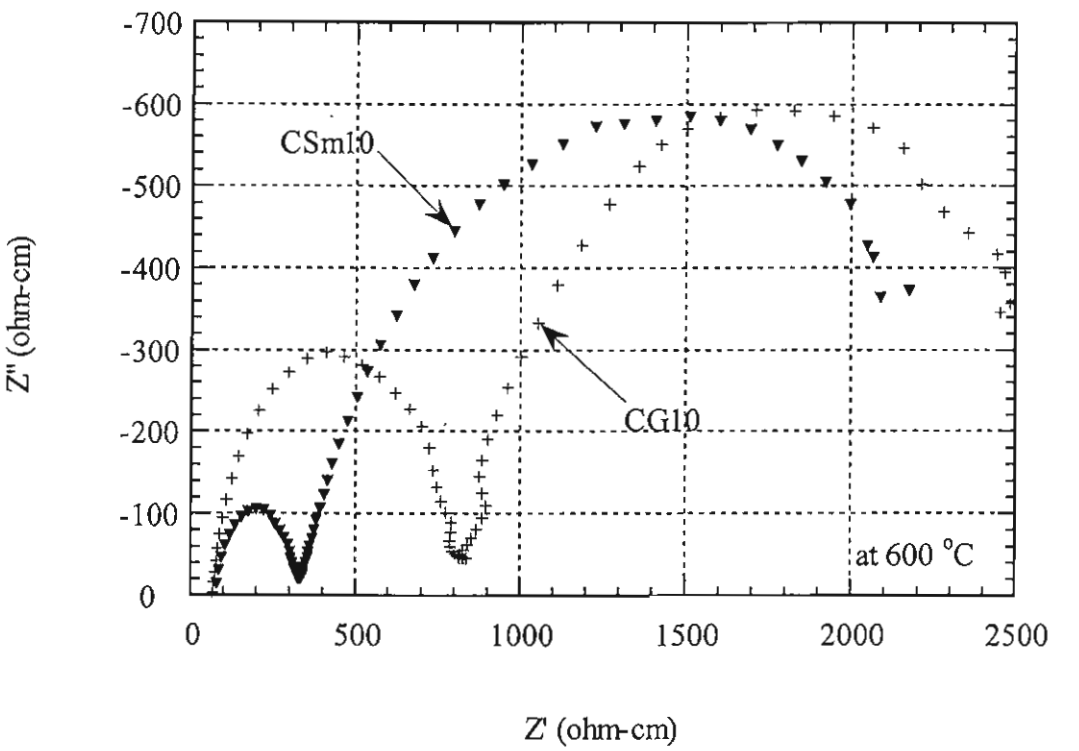

Fig. 23 Impedance spectra for CG10 and CSm10 sintered at 1500 °C for 2 hrs

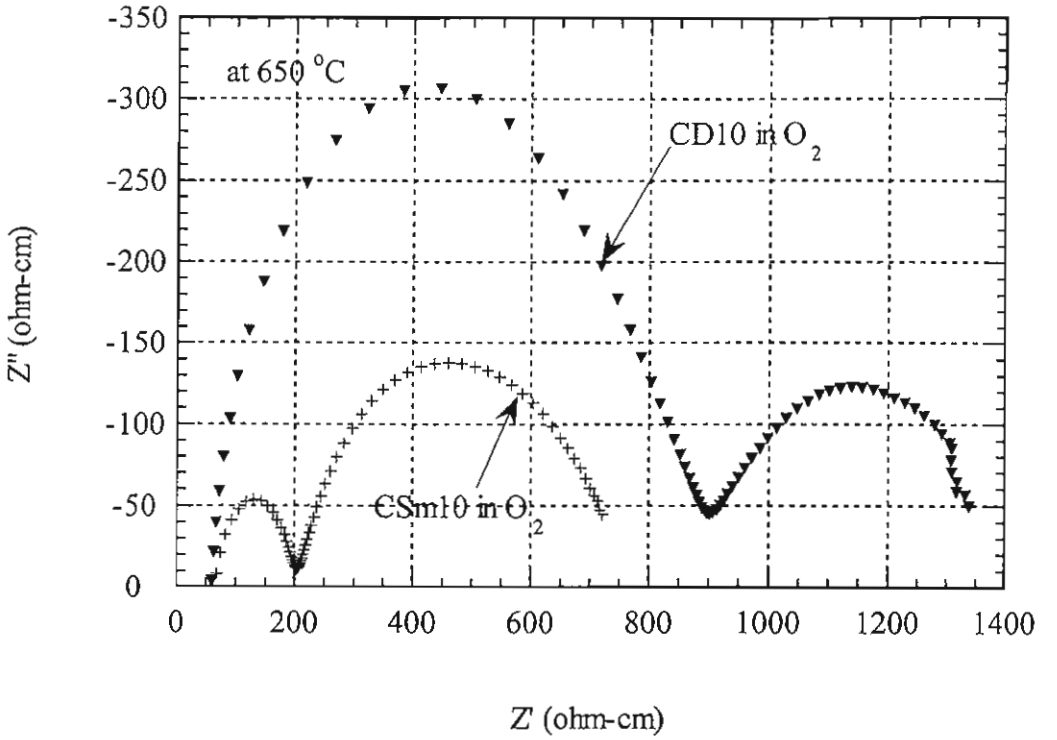

Fig. 24 Impedance spectra for CD10 and CSm10 sintered at 1500 °C for 2 hrs

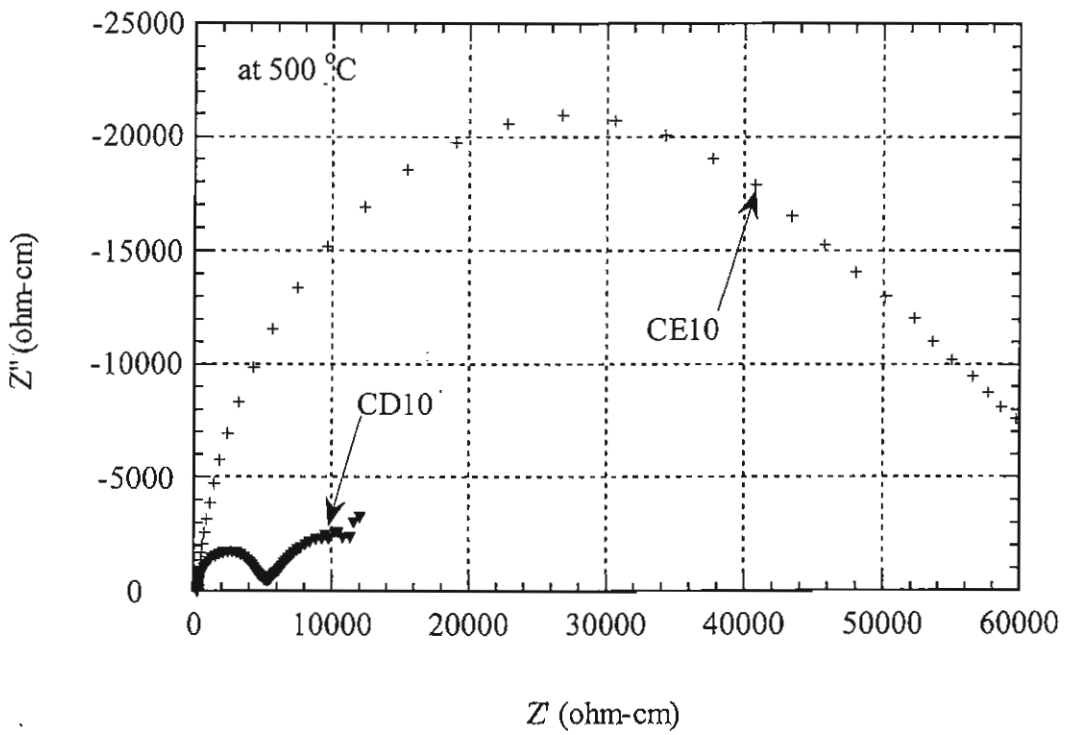

Fig. 25 Impedance spectra for 10 mol% Dy- and 10 mol% Er- doped CeO_2

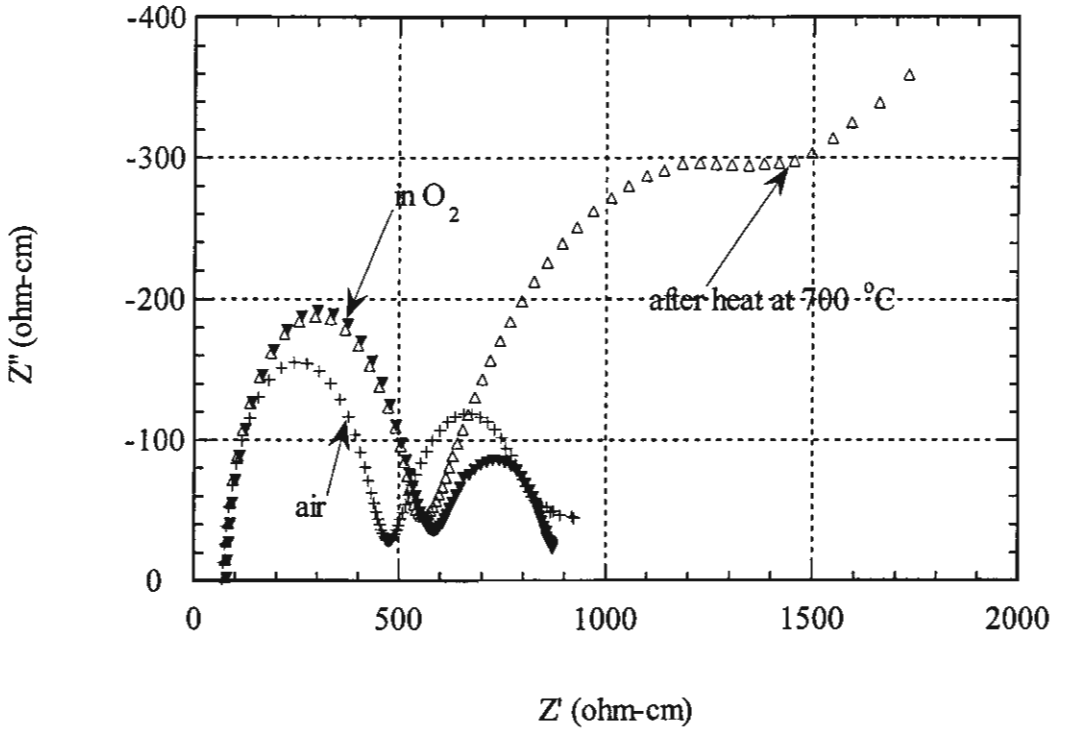

Fig. 26 Impedance spectra for 20 mol% Er-doped ceria measurement at 650 °C

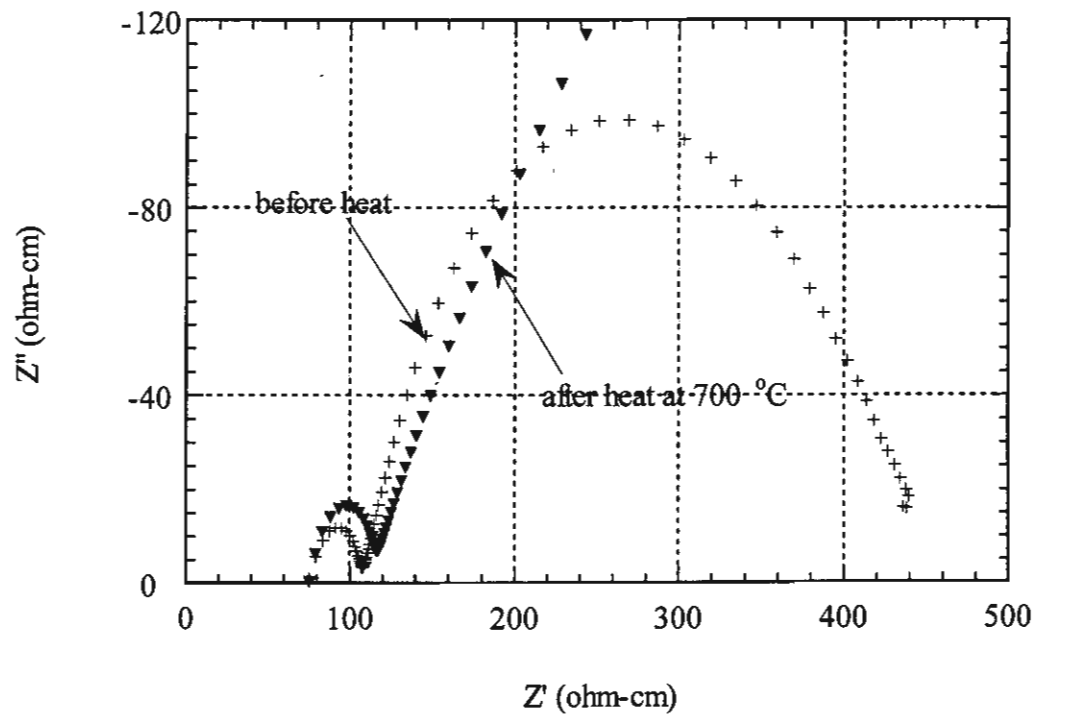

Fig. 27 Impedance spectra for 30 mol% Gd- doped CeO_2 measurement at 650 °C

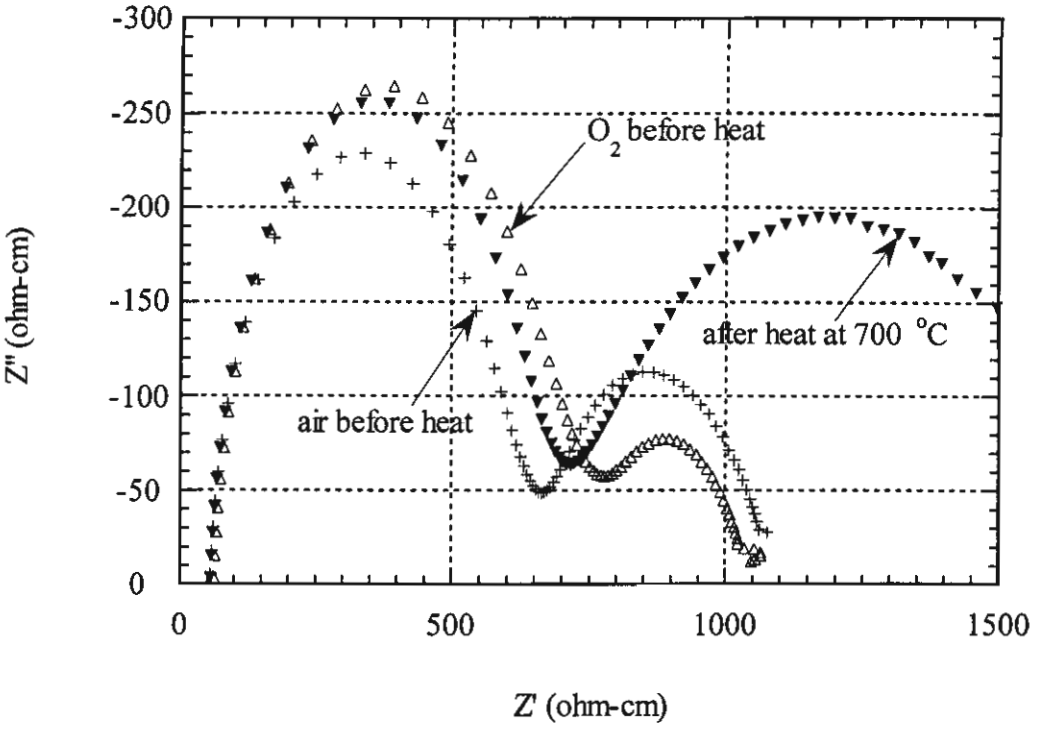

Fig. 28 Impedance spectra for 20 mol% Y- doped CeO_2 measurement at 650 °C

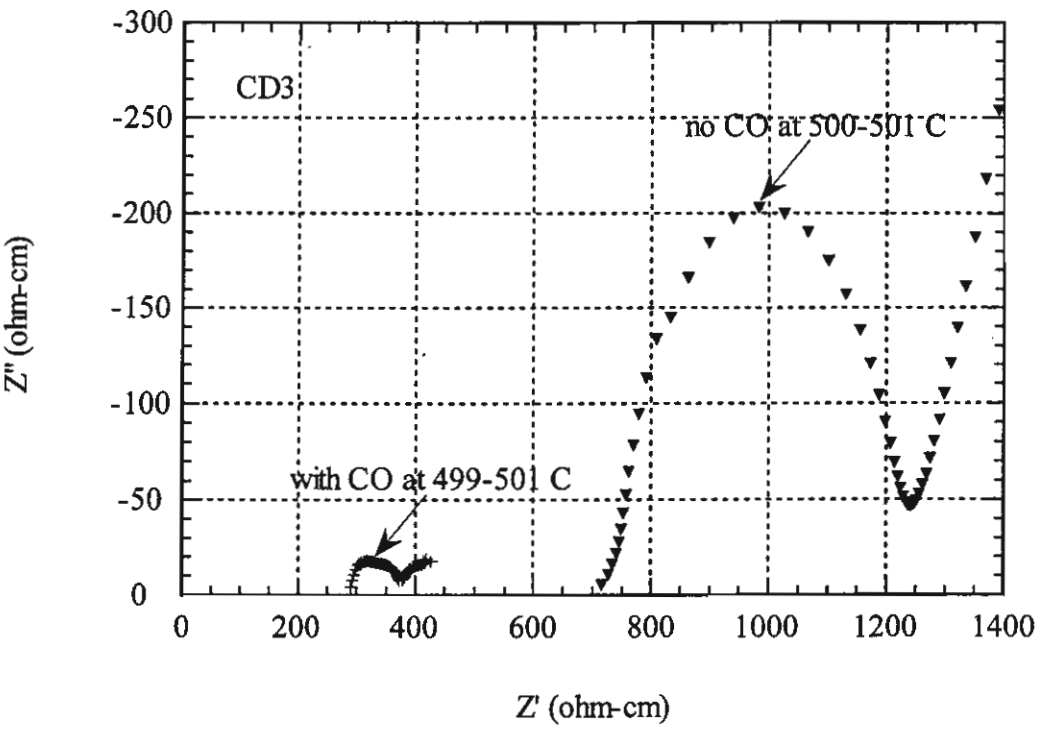

Fig. 29 Impedance spectra of $Ce_{0.7}Dy_{0.3}O_{2-x}$ measured with and without CO

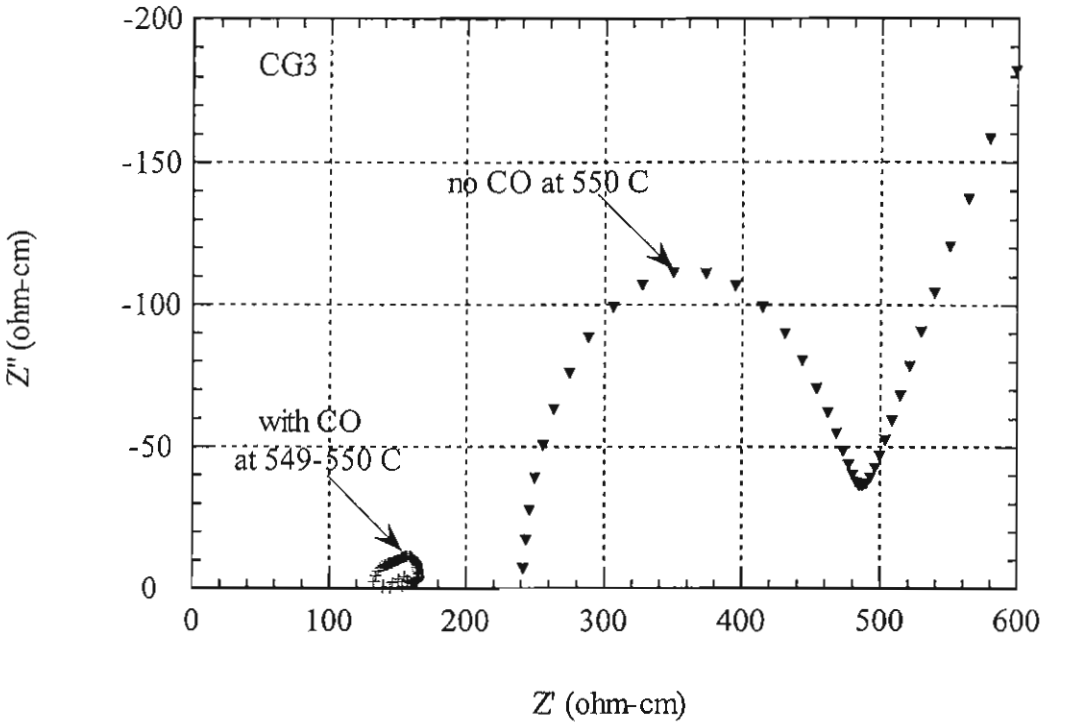

Fig. 30 Impedance spectra of $Ce_{0.7}Gd_{0.3}O_{2-x}$ measured with and without CO

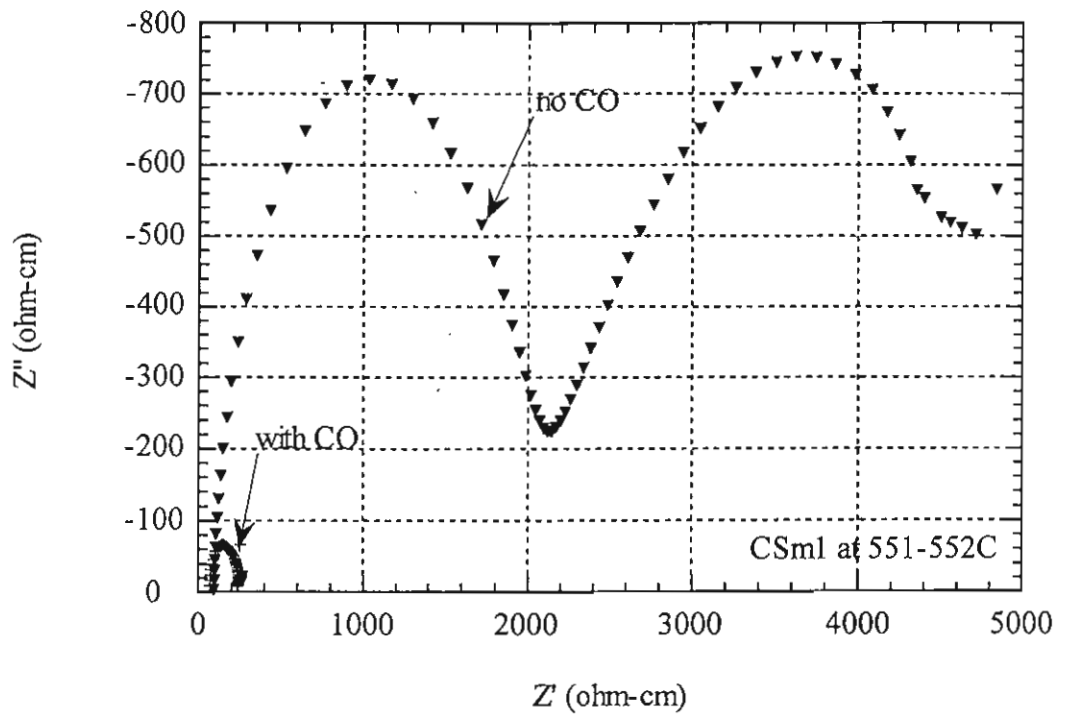

Fig. 31 Impedance spectra of $Ce_{0.9}Sm_{0.1}O_{2-x}$ measured with and without CO

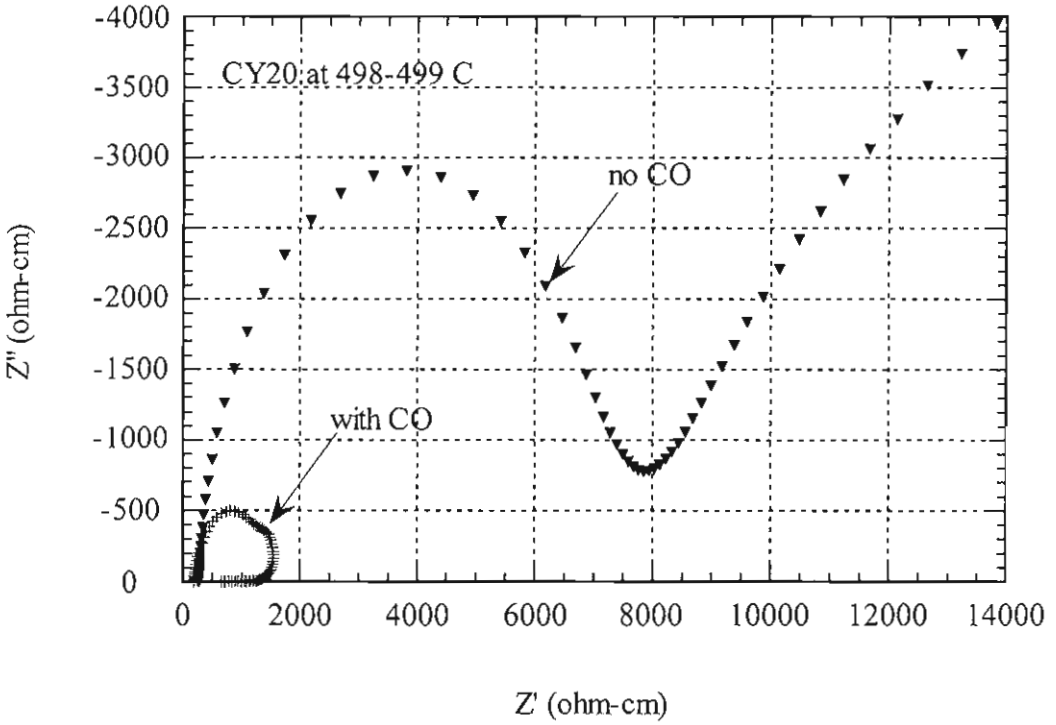

Fig. 32 Impedance spectra of $Ce_{0.8}Y_{0.2}O_{2-x}$ measured with and without CO

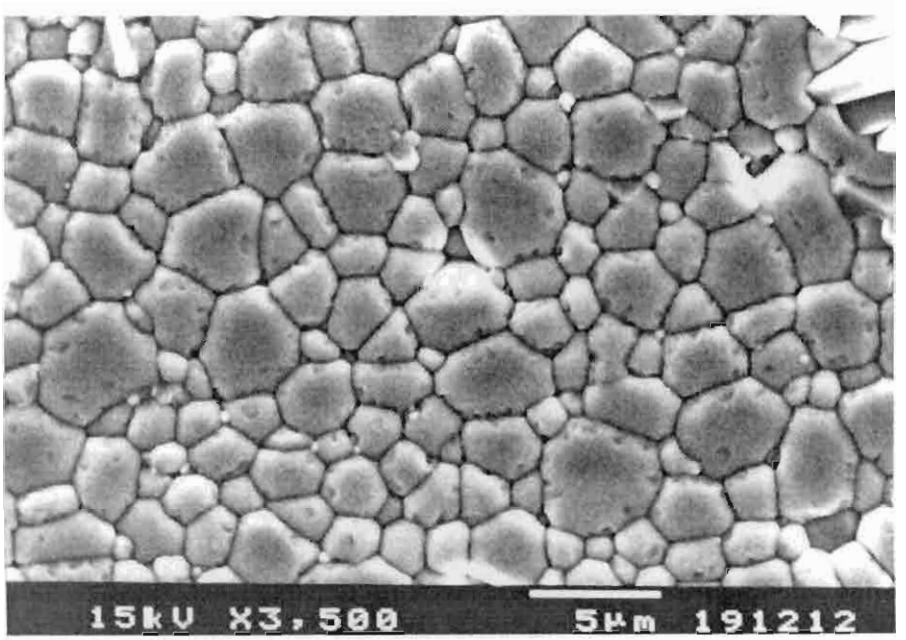

Fig. 33 SEM of sintered $Ce_{0.8}Dy_{0.2}O_{2-x}$ at 1500 °C for 5 hrs after heat at 700 °C 90 hrs

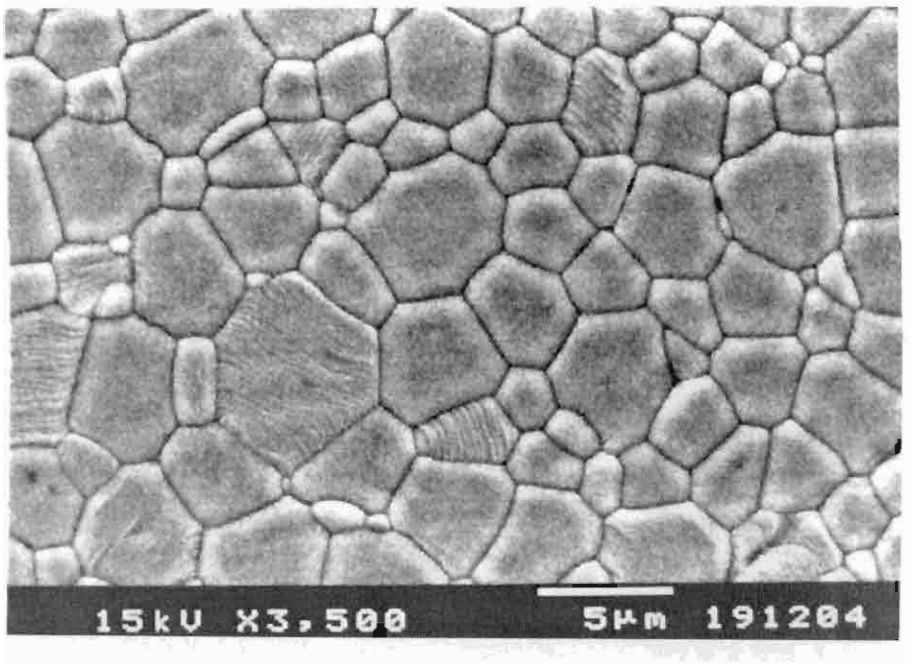

Fig. 34 SEM of sintered $Ce_{0.7}Dy_{0.3}O_{2-x}$ at 1500 °C for 5 hrs after heat at 700 °C 90 hrs

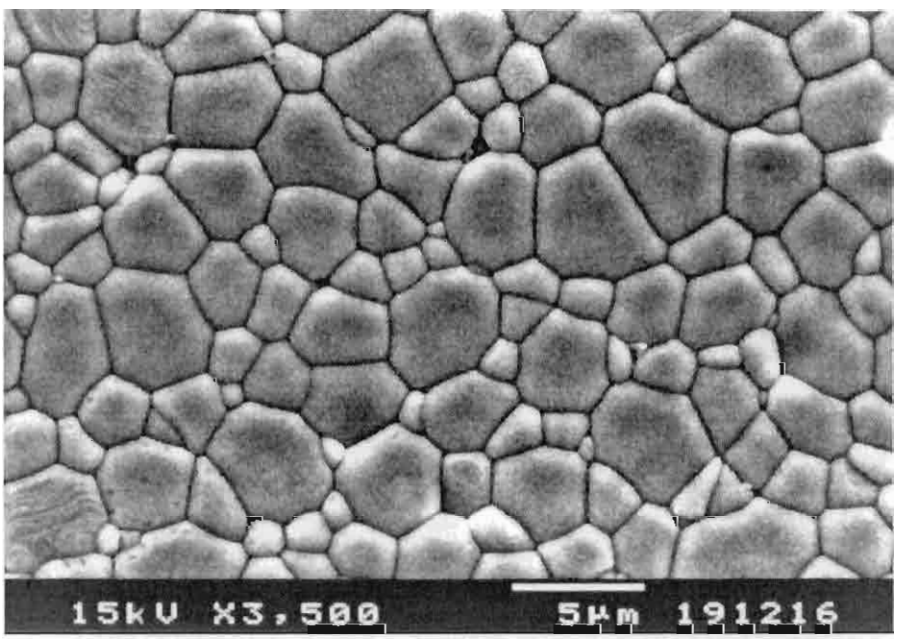

Fig. 35 SEM of sintered $Ce_{0.8}Er_{0.2}O_{2-x}$ at 1500 °C for 5 hrs after heat at 700 °C 90 hrs

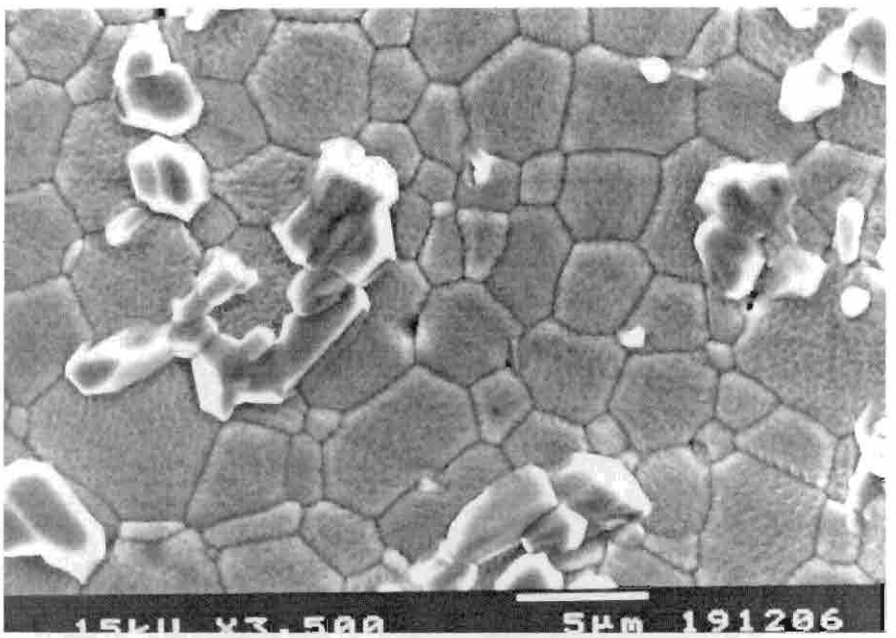

Fig. 36 SEM of sintered $Ce_{0.7}Gd_{0.3}O_{2-x}$ at 1500 °C for 10 hrs after heat at 700 °C 90 hrs

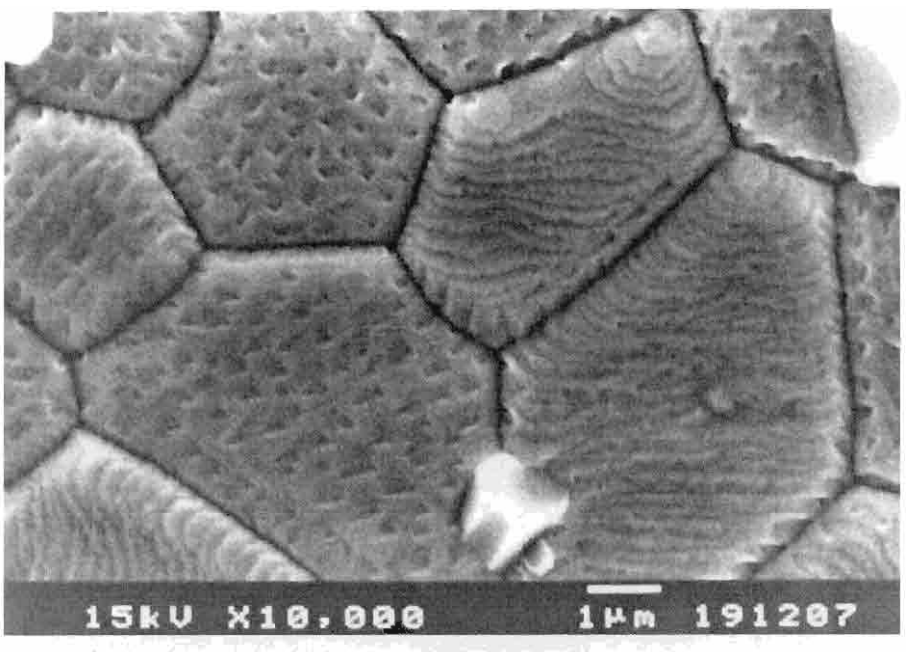

Fig. 37 SEM of etching pitch of sintered $Ce_{0.7}Gd_{0.3}O_{2-x}$ at 1500 °C for 10 hrs after heat

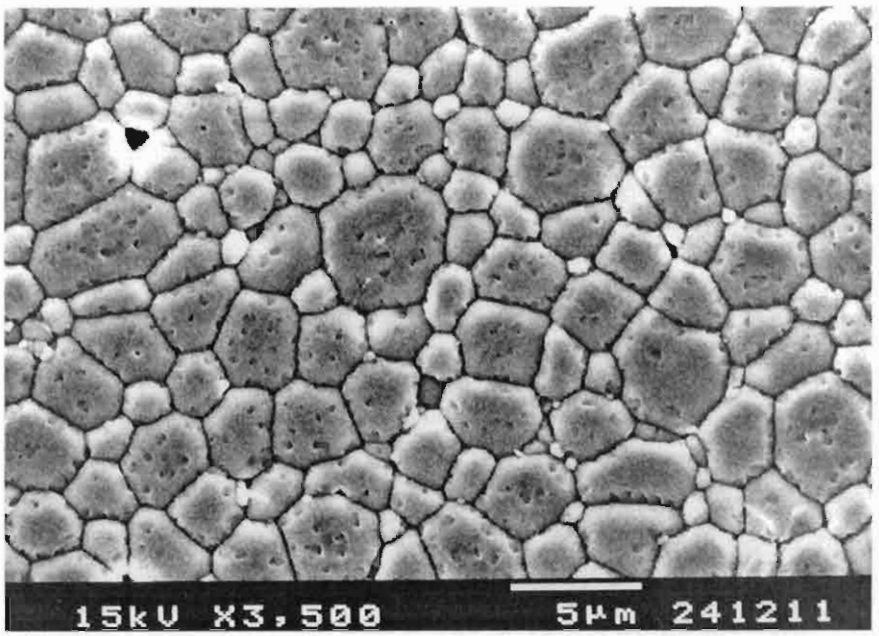

Fig. 38 SEM of sintered $Ce_{0.9}Sm_{0.1}O_{2-x}$ at 1500 °C for 2 hrs after heat at 700 °C 90 hrs

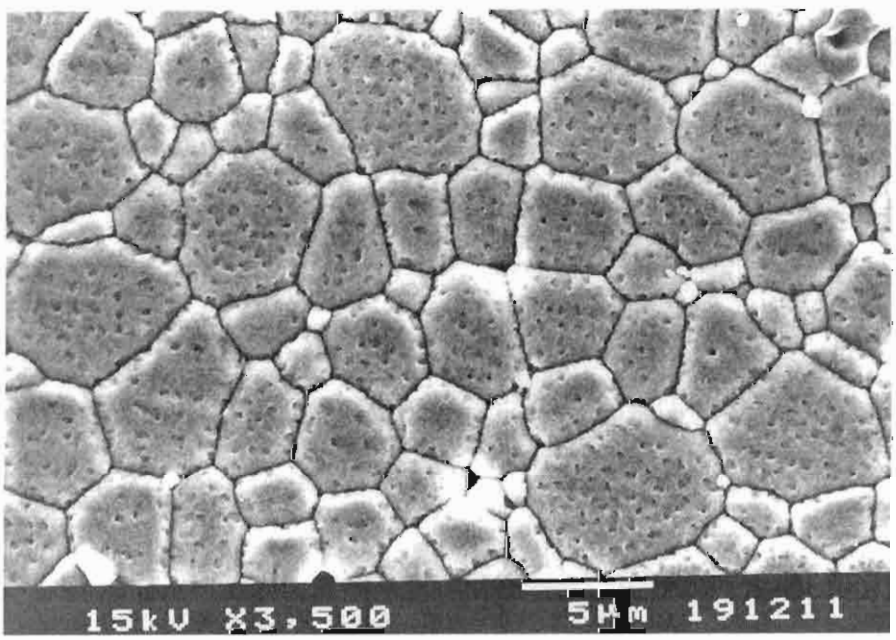

Fig. 39 SEM of sintered $Ce_{0.9}Sm_{0.1}O_{2-x}$ at 1500 °C for 5 hrs after heat at 700 °C 90 hrs

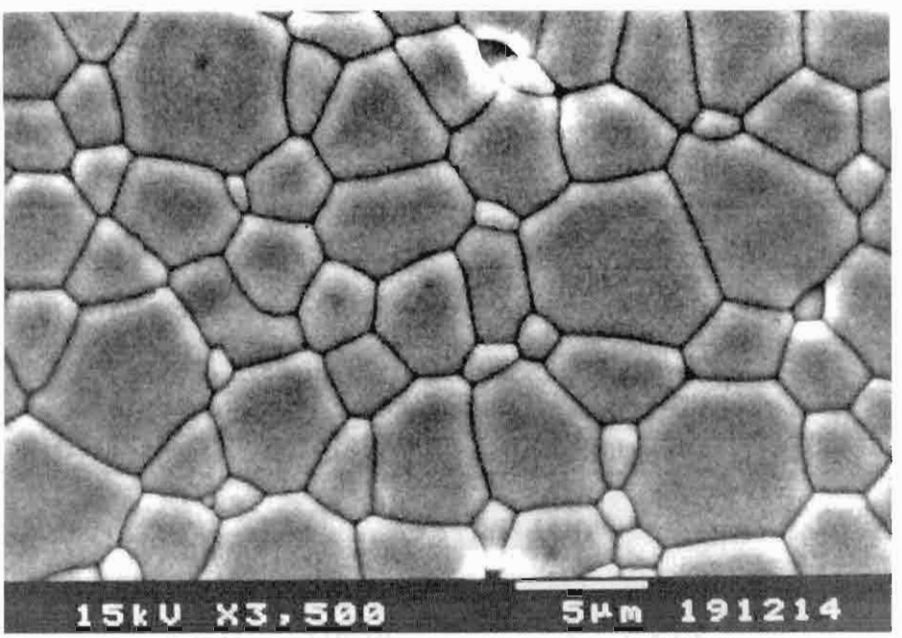

Fig. 40 SEM of sintered $Ce_{0.8}Y_{0.2}O_{2-x}$ at 1500 °C for 10 hrs after heat at 700 °C 90 hrs

References

[1]. K. Huang and J.B. Goodenough, "A solid oxide fuel cell based on Sr- and Mg-doped $LaGaO_3$ electrolyte: the role of a rare-earth oxide buffer," J. Alloys and Compounds **303-304** (2000) 454-464.

[2]. H. Ullmann, N. Trofimenko, A. Naoumidis and D. Stover, "Ionic/electronic Mixed Conduction Relations in Perovskite-type Oxides by Defect Structure," J. European Ceram. Soc. **19** (1999) 791-796.

[3]. J. W. Stevenson, T.R. Armstrong, L.R. Pederson, J. Li, C.A. Lewinsohn and S. Baskaran, "Effect of A-site cation nonstoichiometry on the properties of doped lanthanum gallate," Solid State Ionics **113-115** (1998) 571-583.

[4]. B.C.H Steele in: High Conductivity Solid Ionic Conductors, T. Takahashi (Ed.), World Scientific, Singapore (1989).

[5]. A. Trovarelli, "Catalysis by Ceria and Related Materials", in Catalytic Science Series, Vol. 2, Imperial College Press (2002).

[6]. M. Mogensen, N. M. Sammes and G. A. Tompsett, "Physical, chemical and electrochemical properties of pure and doped ceria," Solid State Ionics **129** (2000) 63-94.

[7]. G. B. Balazs, R. S. Glass, "as impedance studies of rear earth oxide doped ceria," Solid State Ionics **76** (1995) 155-162.

[8]. K. Eguchi, T. Setoguchi, T. Inoue and H. Arai, "Electrical properties of ceria-based oxides and their application to solid oxide fuel cells," Solid State Ionics **52** (1992) 165-172.

[9]. D. R. Lide in: Handbook of Chemistry and Physics, **73rd** Ed. CRC Press (1992).

[10]. B.C.H Steele, "Appraisal of $Ce_{1-y}Gd_yO_{2-y/2}$ electrolytes for IT-SOFC operation at 500 °C," Solid State Ionics **129** (2000) 95-110.

[11]. L. Minervini, M.O. Zacate and R.W. Grimes, "Defect cluster formation in M_2O_3 – doped CeO_2," Solid State Ionics **116** (1999) 339-349.

[12]. T. Mori, J. Drennan, J-H Lee, J-G Li and T. Ikegami, "Oxide ionic conductivity and microstructures of Sm- or La-doped CeO_2 –based systems," Solid State Ionics **154-155** (2002) 461-466.

[13]. N. Maffei and A. K. Kuiakose, "Solid oxide fuel cells of ceria doped with gadolinium and praseodymium," Solid State Ionics **107** (1998) 67-71.

[14]. L.L. Hench and J.K. West in: Principles of Electronic Ceramics, John Wiley & Sons (1990) 7.

[15]. C. Gabrielli in: Physical Electrochemistry, I. Rubinstein (Ed.), Marcel Dekker, Inc. (1995).

[16]. N. Bonanos, B. C. H. Steele and E. P. Butler in: Impedance Spectroscopy emphasizing solid materials and systems, J. R. Macdonald (Ed.), John Wiley & Sons (1987).

[17]. Zplot for Windows in Electrochemical Impedance Software Operating Manual, Scribner Associates, Inc.

[18]. K. Huang, M. Feng and J. B. Goodenough, "Synthesis and Electrical Properties of Dense Ce 0.9 Gd 0.1 O 1.95 Ceramics," J. Am. Ceram. Soc. **81** (1998) 357-362.

[19]. D.Y. Wang and A.S. Nowick, "The grain-boundary effect in doped ceria solid electrolytes," J. Solid State Chem. **35** (1980) 325-333.

Appendix A

JCPDS #34-0394

34-0394

CeO2

Cerium Oxide

Cerianite-(Ce), syn

Rad.: CuKa1 λ: 1.5405 Filter: Graph Mono d-sp: Diffractometer

Cut off: 22.1 Int.: Diffract. I/Icor.:

Ref: Natl. Bur. Stand. (U.S.) Monogr. 25, 20, 38 (1983)

Sys.: Cubic S.G.: Fm3m (225)

a: 5.41134(12) b: c: A: C:

α: β: γ: Z: 4 mp:

Ref: Ibid.

Dx: 7.215 Dm: SS/FOM$_{16}$=130(.0077, 16)

Color: Light gray, yellowish brown
Peak height intensity. Pattern taken at 26(1) C. CAS #: 1306-38-3. This yttria stabilized phase was prepared at NBS, Gaithersburg, MD, USA, by Dragoo, Domingues (1982) from co-precipitation of the oxides. The powder was calcined at 620 C and then formed into a billet without binder, isostatically pressed, and then hot-pressed in an alumina die for 30 minutes at 1350 C with an applied stress of 28 MPa. The structure of fluorite was determined by Bragg (1914). Ca F2 type. Fluorite group, uraninite subgroup. Also called: ceria.Silver used as an internal stand. PSC: cF12. To replace 4-593. Mwt: 172.12. Volume[CD]: 158.46.

2θ	Int	h	k	l
28.555	100	1	1	1
33.082*	30	2	0	0
47.479*	52	2	2	0
56.335*	42	3	1	1
59.087*	8	2	2	2
69.402*	8	4	0	0
76.700*	14	3	3	1
79.070*	8	4	2	0
88.412*	14	4	2	2
95.397*	11	5	1	1
107.265	4	4	4	0
114.730	13	5	3	1
117.318	6	6	0	0
128.393	9	6	2	0
137.972	6	5	3	3
141.568	5	6	2	2

Appendix B

Chemical Reagent Used in Synthesis

Bismuth (III) Oxide, Bi_2O_3	99.9%	Kanto Chemical Company, Inc.
Cerium (IV) Oxide, CeO_2	99.9%	Aldrich Chemical Company, Inc.
Dysprosium (III) Oxide, Dy_2O_3	99.9%	Aldrich Chemical Company, Inc.
Erbium (III) Oxide, Er_2O_3	99.9%	Aldrich Chemical Company, Inc.
Gadolinium (III) Oxide, Gd_2O_3	99.9%	Aldrich Chemical Company, Inc.
Gold, GG501	9%Au	Cerdec AG Ceramic Colours
Iron (III) Oxide, Fe_2O_3	99+%	Aldrich Chemical Company, Inc.
Lanthanum Oxide, La_2O_3	99.9%	Aldrich Chemical Company, Inc.
Samarium (III) Oxide, Sm_2O_3	99.9%	Aldrich Chemical Company, Inc.
Strontium Carbonate, $SrCO_3$	99.9+%	Aldrich Chemical Company, Inc.
Stannous Oxide, SnO		Baker Analyzed
Yttrium Oxide, Y_2O_3	99.99%	Kanto Chemical Company, Inc.

Output from this Project

1. **Publication:** Sutin Kuharuangrong, "**Effects of Ni on the electrical conductivity and microstructure of $La_{0.82}Sr_{0.16}MnO_3$,**" Ceramics International **30** (2004) 273-277.
2. **Cooperation with MTEC** researchers and SOFC projects at the present time and in the future.

ELSEVIER

Ceramics International 30 (2004) 273–277

CERAMICS INTERNATIONAL

www.elsevier.com/locate/ceramint

Effects of Ni on the electrical conductivity and microstructure of $La_{0.82}Sr_{0.16}MnO_3$

Sutin Kuharuangrong

School of Ceramic Engineering, Suranaree University of Technology, Nakhon Ratchasima 30000, Thailand

Received 17 January 2003; received in revised form 24 March 2003; accepted 28 April 2003

Abstract

The effects of Ni doped into $La_{0.82}Sr_{0.16}MnO_3$ (LSM) have been studied. $La_{0.82}Sr_{0.16}Mn_{1-x}Ni_xO_3$ compositions with Ni content up to $x=0.3$ have been prepared by the solid state reaction and characterized to investigate the microstructure, thermal expansion coefficient (TEC) and electrical conductivity. A second phase detected by X-ray diffractometry has been found in all compositions after sintering at 1470 °C for 2 h. The results from scanning electron microscope show that the grain sizes of LSM reduce with Ni content and its TEC is changed insignificantly by Ni. The TEC value of 11.7×10^{-6} K^{-1} between 100 and 900 °C is obtained for $0\leqslant x\leqslant0.3$. The electrical conductivity from dc four point measurement indicates a trend of decreasing conductivity with increasing Ni content.

Keywords: C. Electrical conductivity; D. Perovskites

1. Introduction

Lanthanum strontium manganite (LSM) has been extensively studied as cathode for solid oxide fuel cell (SOFC). An increasing amount of Sr enhances the electrical conductivity of $LaMnO_3$ due to the increasing concentration of Mn^{4+}. However, Sr raises the thermal expansion coefficient (TEC) of $LaMnO_3$ resulting in mismatch with those of other components of SOFC. The composition of $LaMnO_3$ with 15–20 mol% strontium [1–4] is commonly used to investigate its properties. In addition, other divalent cations such as Ca, Mg and Ba are used to dope into A-site of this perovskite oxide, ABO_3. However, only Cr, Co and Ni have been usually selected for substitution on the B-site of LSM [5,6]. Co and Ni decrease the electrical conductivity of $La_{0.5}Sr_{0.5}MnO_3$ [5]. In contrast, Liu et al. [6] have reported that the addition of 0.1 mole fraction of Ni into Mn-site increases the electrical conductivity of $La_{0.6}Sr_{0.4}MnO_3$ but decreases that of $La_{0.82}Sr_{0.2}MnO_3$. This paper attempts to investigate the effect of Ni on the electrical conductivity of $La_{0.82}$ $Sr_{0.16}MnO_3$ including the microstructure and the thermal expansion coefficient. $La_{0.82}Sr_{0.16}MnO_3$ is selected to be lanthanum-deficient based composition for this work to enhance the chemical stability for the reactivity reduction of LSM toward YSZ electrolyte. The addition of 10, 20 and 30-mole% Ni as a dopant in this composition has been examined and properties compared with undoped material.

2. Experimental procedure

All compositions of undoped and Ni-doped $La_{0.82}Sr_{0.16}MnO_3$ were synthesized from La_2O_3, $SrCO_3$, Mn_2O_3 and NiO by solid state reaction route. 10, 20 and 30- mole% Ni were added and expected to substitute in Mn-site due to the similar ionic size. The total amount of cations on the B-site of perovskite oxide ABO_3 was one. The following abbreviation was used to identify each composition:

LSM for $La_{0.82}Sr_{0.16}MnO_3$,
LSMN1 for $La_{0.82}Sr_{0.16}Mn_{0.8}Ni_{0.1}O_3$,
LSMN2 for $La_{0.82}Sr_{0.16}Mn_{0.8}Ni_{0.2}O_3$ and
LSMN3 for $La_{0.82}Sr_{0.16}Mn_{0.7}Ni_{0.3}O_3$

E-mail address: sutin@ccs.sut.ac.th (S. Kuharuangrong).

0272-8842/03/$30.00
doi:10.1016/S0272-8842(03)00099-3

Before weighing, La_2O_3 raw material was calcined at 1000 °C to decompose either hydroxide or carbonate of lanthanum and the others were used as received. The non-stoichiometric compositions were prepared by milling with absolute ethanol in a polypropylene bottle. After drying, the mixture was calcined in air and the maximum firing temperature including the soaking temperatures during calcination were determined by differential thermal analysis (DTA, Perkin-Elmer DTA7). The phase of calcined powder was analyzed by X-ray diffraction (XRD, Jeol JDX3530). In addition, the lattice parameter was determined after correction of peak shift error in d-spacing with an addition of silicon as an internal standard. Disk or bar-shaped specimens were obtained after grinding and pressing the calcined powder. All compositions were sintered in air at 1470 °C for 2 h. The phase of fired samples was characterized by XRD to investigate any phase change after sintering.

The effect of Ni on the thermal expansion coefficient (TEC) of LSM was investigated by dilatometer (Netzsch, DIL402C). The data were collected from room temperature to 1000 °C with a heating rate of 3 °C/min.

The electrical conductivity of sintered bars using a dc four point method was measured as a function of temperature. Fired-on gold electrode was applied on the specimens before measurement. The data were collected from 100 to 900 °C with an increasing temperature of 3 °C/min.

The microstructure of sintered compositions was observed by scanning electron microscope (SEM, Jeol JSM5410LV). The samples were polished and thermally etched before examination.

3. Results and discussion

The results of differential thermal analysis for the mixed raw materials of LSM and LSMN3 compositions are represented in Fig. 1. The data show that the first two reactions occur in the range of 300–420 °C and 520–570 °C for both of LSM and LSMN3. However, the last reaction appears in different temperature ranges, 950–975 °C for LSM but 820–870 °C for LSMN3. Although the reactions from these results were complete before 1000 °C, the mixed powder of each composition in this work was calcined at the maximum temperature of 1200 °C and held at the temperatures which the reaction peaks occurred to obtain a uniform single phase. Fig. 2 shows the X-ray powder patterns of $La_{0.82}Sr_{0.16}Mn_{1-x}Ni_xO_3$ for $0 \leqslant x \leqslant 0.3$ after calcining at 1200 °C. The results indicate these compositions exhibit the characteristic pattern of a distorted orthorhombic crystal structure since the angle is close to 90°. There is no evidence of a second phase in the patterns. The calculated lattice parameters of all compositions after correction of peak shift are also listed in Table 1. The results show that with an increasing amount of Ni substituted into Mn, the lattice parameters of LSM decrease.

Fig. 3 shows the XRD patterns of undoped and doped LSM after sintering at 1470 °C for 2 h. The results exhibit the same phase present as revealed in Fig. 2. However, the appearance of a small peak at

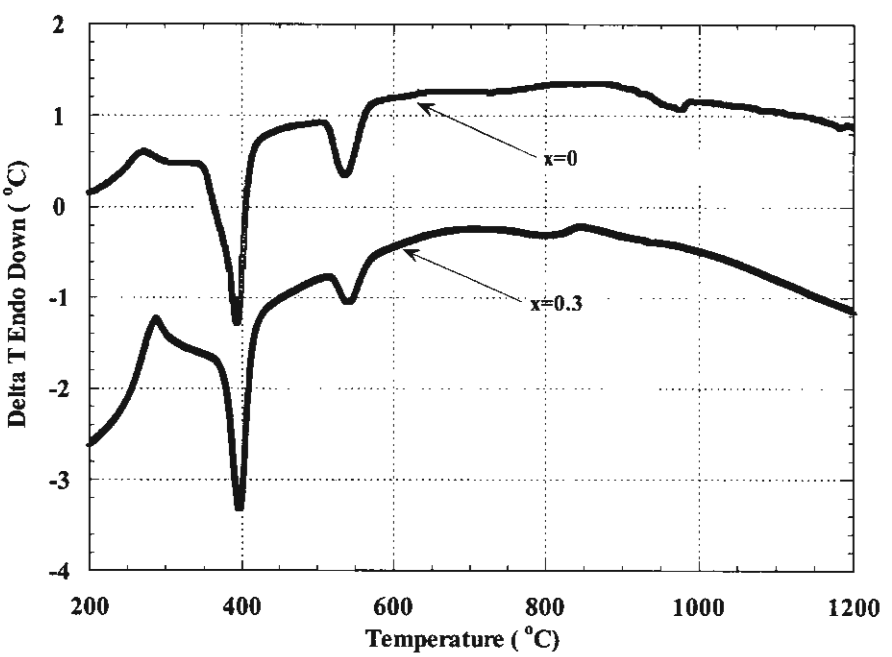

Fig. 1. DTA traces of the mixed raw materials for $La_{0.82}Sr_{0.16}Mn_{1-x}Ni_xO_3$.

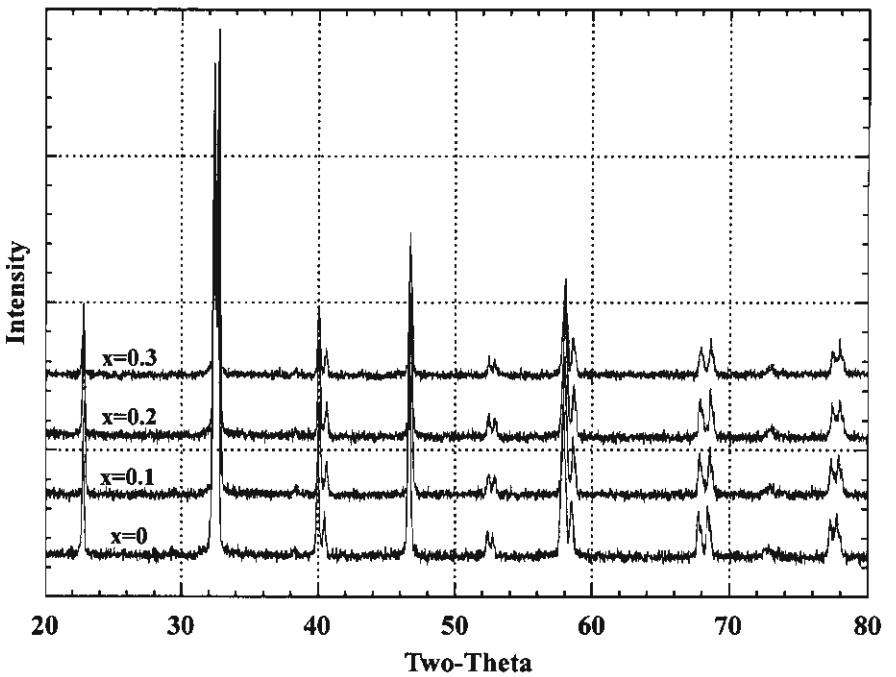

Fig. 2. XRD patterns of $La_{0.82}Sr_{0.16}Mn_{1-x}Ni_xO_3$ powder after calcining at 1200 °C.

Table 1
Calculated lattice parameter of LSM as a function of Ni concentration

Compositions	Lattice parameter (Å)		
	a	*b*	*c*
LSM	5.478	5.529	7.772
LSMN1	5.476	5.526	7.771
LSMN2	5.467	5.522	7.770
LSMN3	5.460	5.503	7.768

Table 2
Thermal expansion coefficient (TEC), the electrical conductivity at 900 °C and the activation energy as a function of Ni concentration

Composition	$TEC_{100-900\ °C}$ ($\times 10^{-6}\ K^{-1}$)	Conductivity	
		$\sigma_{900\ °C}$ (S/cm)	E_a (kJ/mol)
LSM	11.7	107	12.9
LSMN1	11.5	92	16.1
LSMN2	11.7	68	15.8
LSMN3	11.8	48	18.0

$2\theta \approx 44.5°$ as pointed by the arrow could be observed in all sintered compositions. This suggests a second phase being possibly present after sintering at high temperature.

The effect of Ni-doped LSM on the thermal expansion coefficient (TEC) can be observed in Table 2. The experimental data measured from 100 to 900 °C indicate that the concentration of Ni does not have an influence on the expansion of LSM. The average TEC value of LSM and Ni-doped LSM is around $11.7 \times 10^{-6}\ K^{-1}$.

Fig. 4 illustrates the electrical conductivity of sintered compositions as a function of temperature. The data show that LSM has higher electrical conductivity than Ni-doped LSM through all measured temperatures. This is in agreement with the work of Carter et al. [5], in which $La_{0.5}Sr_{0.5}(Mn_{0.8}Co_{0.2})_{0.6}Ni_{0.4}O_3$ was reported to exhibit the lower electrical conductivity than the one without Ni. Nevertheless, the conductivity of the compositions with the lower amount of Ni was not given in the literature. From the result of Fig. 4 the conductivity of undoped LSM at 900 °C is 107 S/cm. With an addition of Ni into LSM, its conductivity decreases and further decreases with an increasing concentration of Ni. The electrical conductivity of Lanthanum manganite generally depends upon the amount of cation dopant with a lower valency and the available sites of Mn^{3+} changed to Mn^{4+}. Therefore, the maximum conductivity with divalent cation dopants on La-site (e.g. Sr, Ca) should occur around 50 mol% dopants since the available sites of Mn^{3+} and Mn^{4+} are equal. In this work, the available sites of Mn^{3+} are reduced attributing to the amount of Ni addition into $La_{0.82}Sr_{0.16}Mn_{1-x}Ni_xO_3$. Furthermore, the lattice parameter calculated from XRD results listed in Table 1 tends to decrease as the amount of Ni dopant increases. The ionic size of Ni^{2+} is larger than that of Mn^{3+} and Mn^{4+} [7]. These suggest that the oxygen vacancies possibly occur in Ni doped $La_{0.82}Sr_{0.16}Mn_{1-x}Ni_xO_{3-\delta}$. The electrons excited from oxygen vacancies may associate with holes hopping from Mn^{4+} to Mn^{3+}, resulting in the decrease of charge carriers. Consequently, the electrical

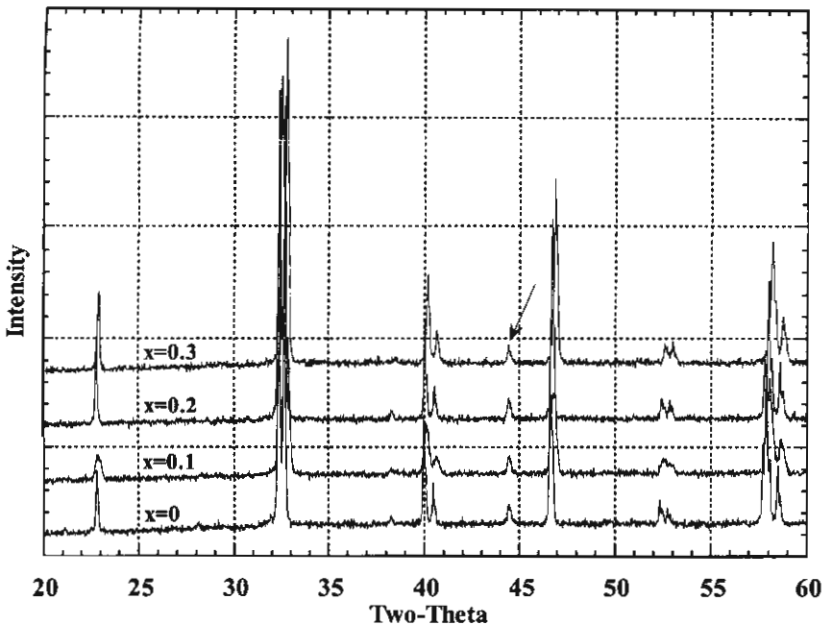

Fig. 3. XRD patterns of $La_{0.82}Sr_{0.16}Mn_{1-x}Ni_xO_3$ specimens after sintering at 1470 °C for 2 h.

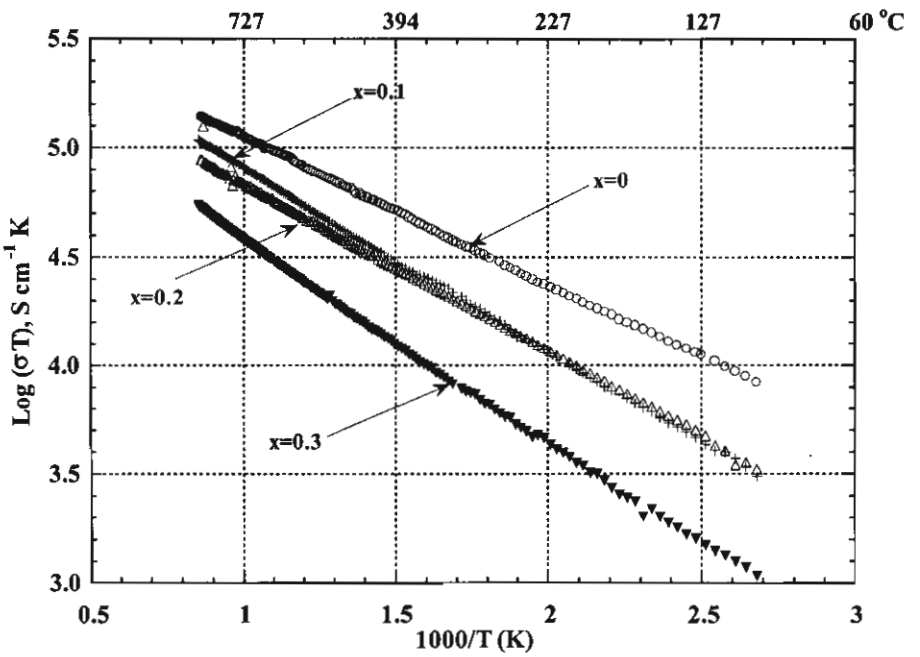

Fig. 4. Arrhenius plots of electrical conductivity of $La_{0.82}Sr_{0.16}Mn_{1-x}Ni_xO_3$.

conductivity of Ni-doped LSM reduces with the amount of Ni. The conductivity at 900 °C and the activation energy of each composition are also given in Table 2. The activation energy obtained from the slope of the data in Fig. 4 tends to increase with the concentration of Ni.

SEM photomicrograph of sintered LSM is shown in Fig. 5a. The average grain size is larger than 15 μm and both intergranular and intragranular pores could be observed in this composition. With Ni dopant, the grain size of LSM decreases with the increasing amount of Ni, resulting in a reduction of the intragranular pores as illustrated in Fig. 5b–d. It should be noted that the magnifications used for LSMN2 and LSMN3 are different from the others. Evidently, the grain size of Ni-doped LSM decreases, thus reducing the surface

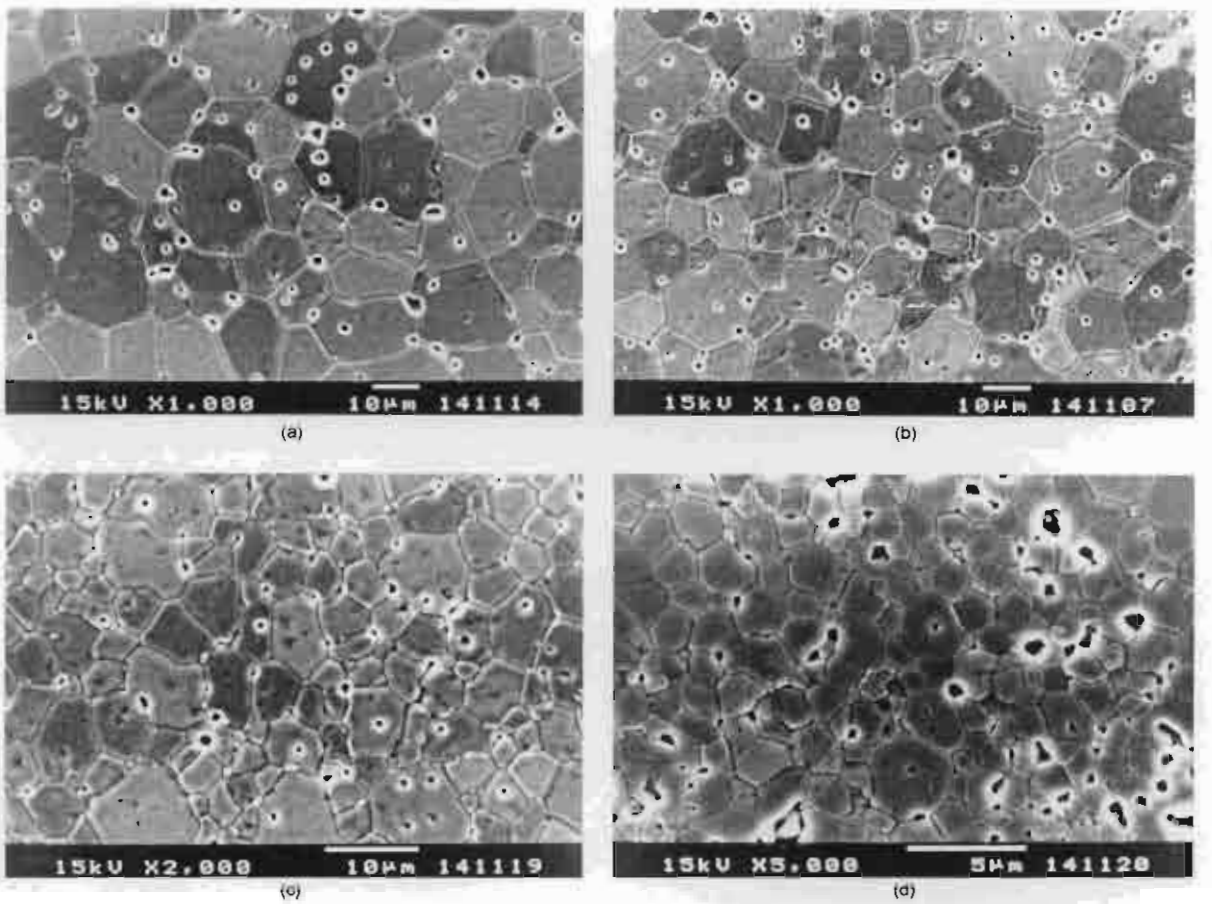

Fig. 5. SEM photomicrographs of compositions sintered at 1470 °C: (a) LSM, (b) LSMN1, (c) LSMN2, (d). LSMN3.

area. This effect is possibly related to the data of electrical conductivity, in which smaller grain size may also affect the lower conductivity.

4. Conclusions

Substitution of Ni into Mn insignificantly changes the TEC but reduces the electrical conductivity of LSM. As the amount of Ni dopant increases, the conductivity of LSM decreases and its activation energy also tends to increase. Furthermore, Ni inhibits the grain growth of this composition resulting in the decrease of surface area.

Acknowledgements

Financial support from Thailand Research Fund under the contract no. RSA/09/2544 is gratefully acknowledged.

References

[1] C.P. Jacobson, S.J. Visco, L.C. De Jonghe, Thin-film solid oxide fuel cells for intermediate temperature (500-800 °C) operation, Ceram. Trans. 109 (2000) 69–75.
[2] B.C.H. Steele, Survey of materials selection for ceramic fuel cells, II. Cathodes and anodes, Solid State Ionics 86–88 (1996) 1223–1234.
[3] M. Godickemeier, K. Sasaki, L.J. Gauckler, Electrochemical characteristics of cathodes in solid oxide fuel cells based on ceria electrolytes, J. Electrochem. Soc. 144 (1997) 1635–1646.
[4] T. Tsai, S.A. Barnett, Effect of LSM-YSZ cathode on thin-electrolyte solid oxide fuel cell performance, Solid State Ionics 93 (1997) 207–217.
[5] S. Carter, A. Selcuk, R.J. Chater, J. Kajda, J.A. Kilner, B.C.H. Steele, Oxygen transport in selected nonstoichiometric perovskite-structure oxides, Solid State Ionics 53–56 (1992) 597–605.
[6] X. Liu, W.-H. Shih, C. Wang, W. Worrell, Synthesis and characterization of $(La_{1-x}Sr_x)(MnNi_y)O_2$ perovskite as cathode for solid oxide fuel cell, Ceram. Trans. 109 (2000) 185–194.
[7] L.L. Hench, J.K. West, Principles of Electronic Ceramics, John Wiley & Sons, New York, 1990.